Corner bifurcations in non-smoothly forced impact oscillators.

Chris Budd* and Petri T. Piiroinen†

Abstract

Simultaneous impacts of multiple objects in mechanical systems are considered. It will be shown that in some cases the dynamics in a neighbourhood of such events can be explained by piecewise linear two-dimensional maps. These maps give rise to a variety of complex dynamics, which will be analysed. A special emphasis will be put on period-adding cascades.

PACS codes: 02.30.Hg, 02.30.Oz, 02.60.Cb, 46.30.pa

Keywords: piecewise smooth dynamical systems, nonsmooth forcing, multiple impacts, piecewise linear maps

1 Introduction

The dynamics of impacting mechanical systems has been the subject of much recent investigation, as it is known that even very simple systems can have very rich dynamics [1, 2, 3, 4, 5, 11, 15, 16, 18, 22, 25, 30, 31, 32, 35, 36, 37, 39, 38]. An example of such a simple system is the (so-called) single degree of freedom oscillator. This comprises a single particle at a position $u(t)$ the motion of which is governed by a smooth dynamical system. This particle is considered to move in the region $u(t) \geq z(t)$ where $z(t)$ is the location of a (massive) obstacle. If $u(t) = z(t)$ then the particle rebounds with an instantaneous change in its velocity. The obstacle itself may be considered to be moving smoothly, and an important example of an impact oscillator, described in [19], is that of a particle moving under gravity and impacting with a sinusoidally moving table. There is now a comprehensive theory describing the behaviour of these systems, in which we see both periodic and chaotic motions arising, and changing at both smooth bifurcations (saddle-node, period-doubling etc) and non-smooth events such as grazing bifurcations [26, 27] and chattering sequences [8].

However, there are many systems arising in practice in which the motion of the obstacle itself may not be smooth. As an example, consider the situation of a massive basket-ball bouncing on a table. This will have a non-smooth motion due to the impacts with the table. If we now release a (very light) table tennis ball from above the basketball, then the basketball acts as a nonsmoothly moving obstacle

*Department of Mathematical Sciences, University of Bath, BA2 7AY Bath, United Kingdom. email: cjb@maths.bath.ac.uk

†Department of Engineering Mathematics, University of Bristol, BS8 1TR Bristol, United Kingdom. tel: +44(0)117 33 17369, fax: +44(0)117 954 6833, email: petri.piiroinen@bristol.ac.uk (corresponding author)

to the motion of the table tennis ball (which we can consider too light to affect the motion of the basket-ball). The resulting dynamics of the table tennis ball as it impacts with the basket ball is most complex. (This experiment is easy to reproduce, and well worth watching as a demonstration of the subtleties of nonlinear dynamics!)

We can therefore ask, what dynamics might we expect to see in a single-degree of freedom impact oscillator if the position $z(t)$ of the obstacle is a *non-smooth function of time*. Motivated by the discussion above we will, in this paper, consider $z(t)$ to be a *continuous* and *periodic* function of time t, for which there are *corner points* t_k at which $z(t)$ has a discontinuous derivative. A canonical example of such a function is the rectified sine wave

$$z(t) = \kappa + \beta|\sin(\omega t)| \tag{1}$$

for which $t_k = k\pi/\omega$. Our attention will be focused on the cases where the particle at $u(t)$ impacts with the obstacle at $z(t)$ at times t very close to t_k. We will refer to this as a *corner event*. If the dynamical system describing the combined motion of the particle and the obstacle depends of a parameter (say λ), then as λ varies we are likely to see corner events occurring. In particular, if $u(t)$ is moving, and impacting with the obstacle, periodically, then as λ varies we may see one of these impacts occurring at a corner point t_k. We will show in this paper that such a corner event can lead to a significant change in the dynamics of $u(t)$, including the generation of a large number of new periodic orbits of high period. We term this change in behaviour a *corner bifurcation* and the analysis of this will be the main subject of this paper. Remarkably, much of this analysis reduces to a study of two-dimensional piecewise linear discontinuous maps. Similar (one-dimensional) maps were introduced by Keener [24] in studies of the behaviour of excitable media and later investigated by Bressloff and Stark [6] who found complex dynamical behaviour including period-adding sequences. Very similar behaviour is observed at a corner bifurcation.

The remainder of this paper is organised as follows. In Section 2 the impact oscillator, impacts and corner events are defined and a brief review is given of the dynamics of the smooth impact oscillator. In Section 3 the idea of discontinuous forcing is introduced and the dynamics it generates is shown. This is followed by an analysis of the corner event in Section 4, where a set of piecewise two-dimensional linear maps is derived which describe the dynamics close to the event. In Section 5 the dynamics of the derived 2D maps is explored and the nature of the corner bifurcation described. Finally in Section 6 we see how this analysis gives a little more insight into the very complex problem of the impacts of several particles.

2 An overview of impact oscillators

2.1 General systems

In this section we describe the basic behaviour an impact oscillator that comprises a particle at position $u(t)$, with velocity $v(t)$, moving smoothly when not impacting, but which intermittently impacts with an obstacle at position $z(t)$ at which point the motion loses smoothness. For simplicity we will assume that the particle and obstacle move in a line so that $z(t) \leq u(t)$ and interact only through impact. Under the motion induced by the moving obstacle, the particles motion will lie in the

extended phase space

$$S = (u, v, t) \equiv (x, t), \tag{2}$$

where $x = (u, v)$. With the restriction that $z \leq u$ this phase space is bounded the surface Σ

$$\Sigma = \{(x, t) : u = z\}. \tag{3}$$

The surface Σ is locally smooth, but has *corners* on the sets

$$\Gamma_k = \{(x, t) : u = z, t = t_k\}$$

corresponding to the points where the function z loses smoothness.

We will assume that in S the particle moves according to the differential equation

$$\frac{d^2u}{dt^2} + 2\sigma\frac{du}{dt} + k^2u = f(t). \tag{4}$$

The solutions $(u, du/dt, t)$ of this differential equation describe trajectories in S. An *impact* occurs when such a trajectory intersects Σ and a *corner event* when it intersects one of the sets Γ_k.

Away from a corner we can prescribe rules governing the effect of the (instantaneous) impact. The impact does not change the positions of the particle, but does lead to an instantaneous change of its their velocity. A simple restitution model of an impact between the particle and the obstacle is to assume that the velocity of the obstacle does not change, but the relative velocity between the particle and the obstacle is reversed, and reduced by a factor of r (the coefficient of restitution). Thus, if an impact occurs at a time t and the velocity of the particle immediately *before* the impact is v^-, then the velocity v^+ immediately *after* the impact is given by

$$\left(v^+ - dz/dt\right) = -r\left(v^- - dz/dt\right) \quad \text{so that} \quad v^+ = (1 + r)dz/dt - rv^-. \tag{5}$$

This expression is not defined at a corner point as dz/dt is not defined at such points. It is unclear what map should be used here, but we observe that the probability of such events is exceedingly rare. Rather than defining an impact law at such points we will consider the effect on the dynamics of having (well defined) impacts arbitrarily close to the time t_k.

The overall behaviour of the impact oscillators (apart from the special case of impacts with the corners) is thus described by the hybrid motion of the smooth system (4) in S and the impact map (5) on the surface Σ.

2.2 Review of the single particle system

As a starting point for our further analysis we briefly review the dynamics of an unforced harmonically oscillating particle u satisfying the differential equation

$$\frac{d^2u}{dt^2} + u = 0, \quad u > z$$

impacting with a smoothly oscillating wall at $z(t) = \sin(\omega t)$. We take $r = 0.8$ leading to energy loss at each impact and consequently to a dissipative system. This example has been widely studied, see for instance [7, 8, 9, 10] and it is known that u can exhibit periodic or chaotic motion depending upon the value of ω. In Fig. 1(a)

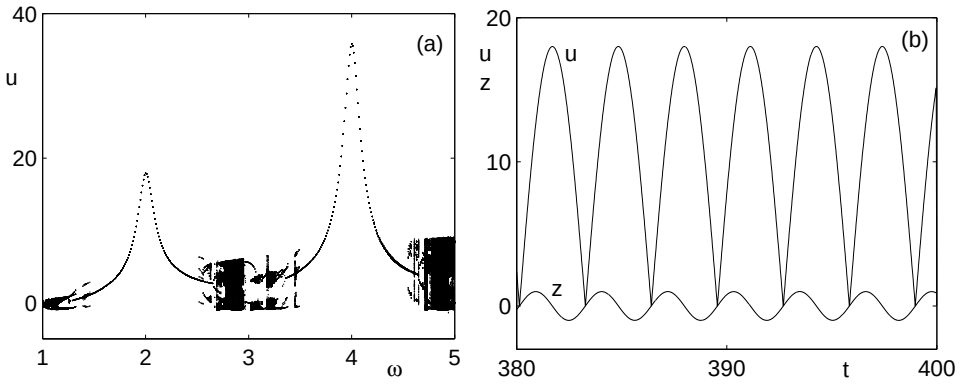

Figure 1: (a) A bifurcation diagram the particle impacting a sinusoidally forced obstacle under frequency variations. (b) A time history of the period-one limit cycle at the resonant frequency $\omega = 2$.

a bifurcation diagram of this case is shown where the position of the particle at the point when the velocity of the particle is equal to the obstacle velocity is plotted, against the oscillating obstacle frequency ω. This diagram, and subsequent bifurcation diagrams in this paper, was obtained by using a direct simulation method. For each value of ω a random set of initial conditions (u, v) was chosen at $t = 0$. The trajectories resulting from each such condition were then computed numerically, with impact points determined by the method of bisection and the impact rule applied at each such point. This process was continued for 500 impacts without plotting and then the dynamics plotted for a further 100 impacts. This was then repeated for other values of ω. This procedure is effective in capturing the range of possible stable asymptotic behaviours of the system, though it will miss unstable behaviour.

In the bifurcation diagram we observe simple (resonant) periodic motion when $\omega = 2$ and $\omega = 4$ surrounded by more complex dynamics, including chaotic behaviour for ω close to 3 and for ω less than 1. Such complex dynamics can arise either through smooth bifurcations, in particular period-doubling bifurcations, or through *grazing* bifurcations which arise when u has a grazing impact with z with $du/dt = dv/dt$. Grazing leads to large local stretching of phase space and is described in detail in [9, 26, 27].
Fig. 1(b) shows a time history of the periodic dynamics at $\omega = 2$. The motion of $u(t)$ in this case takes the form of a rectified sine wave. A brief analysis of this is instructive for understanding the more complex problem with non-smooth forcing. The general motion of $u(t)$ between impacts is given by

$$u(t) = a\cos(t) + b\sin(t).$$

If the obstacle $z(t)$ has frequency $\omega = 2$ and period $T = \pi$ then we seek periodic solutions $u(t)$ of the same period. Let the impact between z and u be at time τ then from the periodicity condition

$$a\cos(\tau) + b\sin(\tau) = a\cos(\tau + \pi) + b\sin(\tau + \pi) = \sin(2\tau).$$

Solving this gives $a = 0$ and $\tau = 0$. The velocity of $u(t)$ just after impact at $t = 0$ is given by

$$v^+(\tau) = -a\sin(\tau) + b\cos(\tau) = b$$

and the velocity v^- just before impact at time $t = \pi$ by $-b$. As the velocity of z at $t = 0$ is $\dot{z} = 2$ it follows from the impact law that

$$b - 2 = -r(-b - 2) \quad \text{so that} \quad b = \frac{2(1+r)}{(1-r)}.$$

The periodic motion of u when $\omega = 2$ can thus be expressed as

$$u(t) = \frac{2(1+r)}{(1-r)} |\sin(t)|. \tag{6}$$

3 Complex dynamics in non-smoothly forced impacting systems

3.1 Problem formulation

We now look at the problem which concerns us for most of this paper, namely the case of non-smooth motion of the obstacle $z(t)$. In the most general case we assume that $z(t)$ is continuous and periodic and at times t_k, dz/dt is discontinuous. Locally, close to t_k the motion of z will be considered to take the form

$$z(t) = \begin{cases} \kappa + \theta_1(t_k - t), & t < t_k, \\ \kappa + \theta_2(t - t_k), & t > t_k, \end{cases} \tag{7}$$

for appropriate values of κ and $\theta_i > 0$. Whilst a wide range of possible functions $z(t)$ could be considered (and will be where possible) we will restrict our attention to the cases where there is single corner in each period. An example of such a function is given by the motion of the particle in the previous section described by the equation (6). Indeed, if the particle considered in this section were a light table tennis ball and the obstacle a basket ball bouncing on a sinusoidally moving table, then $z(t)$ would take precisely this form. To consider a range of (simplest possible) dynamics of the particle u subjected to a periodic, non-smooth forcing it is convenient to generalise the forcing (6) and to consider the parameterised, non-smooth, periodic obstacle motion given by

$$z(t) = \kappa + \beta \left|\sin(\omega t)\right|. \tag{8}$$

In this case we have

$$t_k = k\pi/\omega \quad u(t_k) = \kappa \quad \theta_1 = \theta_2 = \beta\omega.$$

We are now in a position to describe the system that we will study for the remainder of this section and in secs. 4 and 5. For simplicity, we consider the particle u to move in free space between impacts according to the the harmonic equation

$$\frac{d^2u}{dt^2} + u = 0 \quad \text{if} \quad u > z, \tag{9}$$

with impact law (5) arising at the times $t = \tau_j$ when $u = z$ with z given by (8). We will now see that this system has a rich dynamics, rather different from that of the smoothly forced impact oscillator.

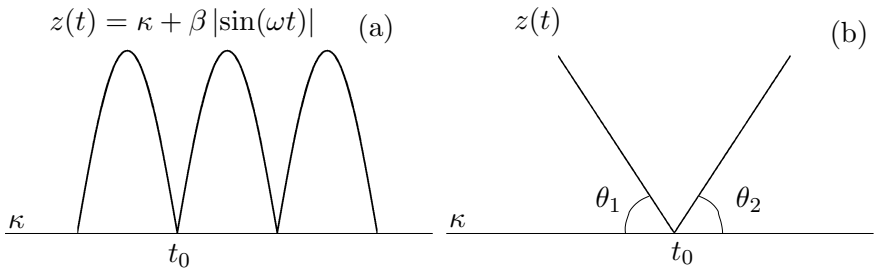

Figure 2: (a) The function $z(t) = \kappa + \beta\,|\sin(\omega t)|$. (b) A magnification of the area in the vicinity of t_0 (cf. eq. (7)).

3.2 Observed dynamics

As parameters in the system, given by (5), (8) and (9), vary we see a change in the various points of impact τ_j between u and z. Under smooth changes in these parameters, there will be values at which u impacts z at a corner point t_k. Fig. 3 shows a schematic of how such a point can be approached at a *corner event*. As τ_j varies through such a point, we see a qualitative different behaviour in the solution and we call the resulting change in the dynamics a *corner bifurcation*. In particular large changes occur in periodic motions with the creation of high period motions. To illustrate these changes, we present in Fig. 4 some simulations of the behaviour of

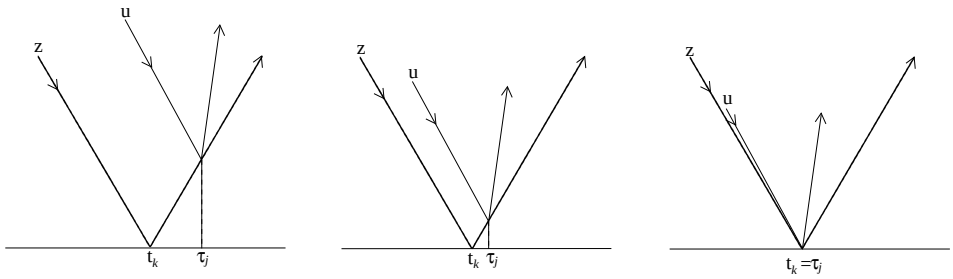

Figure 3: A schematic on how a corner event can locally be approached.

this system by considering the bifurcation diagram of the limit cycles of the motion of u with the non-smooth forcing function (8) taking $\kappa = 0$, $\beta = 1$, $r = 0.8$ and ω treated as the bifurcation parameter.

From the Figs. 4(a) and (b), in which the impact positions are plotted against the frequency, it can be seen that over significant parts of the bifurcation diagram the behaviour of u is periodic with period $T = \pi/\omega$ and with one impact per period. However, as ω is reduced through the point $\omega = \omega_C$, a dramatic change is observed as the point of impact passes through a corner event at time t_C. In the case of $\kappa = 0$ this occurs when $\omega_C = 2$, $t_C = \pi/2$. For ω slightly less than ω_C we then see the co-existence of three distinct types of periodic motion I, II and III, as illustrated in Fig. 5. It is notable that in this case each solution type, with period nT, has $2n$ equivalent solutions but separated with a time shift of $k\frac{\pi}{\omega}$, $k = 0, \cdots, n-1$.

For $\kappa < 0$ a rather different situation is observed. A bifurcation diagram where the frequency $\omega = 1.999$ is kept fixed and κ varied is shown in Fig. 6. When κ is sufficiently large and negative only a simple periodic motion is observed. However,

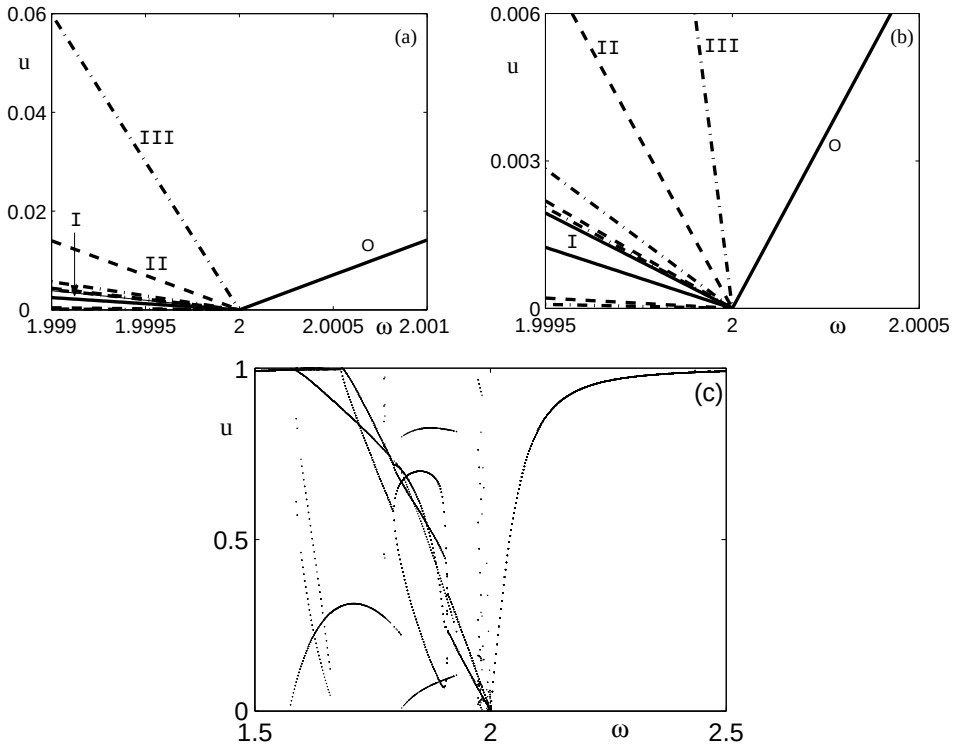

Figure 4: Bifurcation diagrams showing the position of the particle u at impact for $\kappa = 0$ and varying frequency ω. In (a) and (b) the local behaviour in the vicinity of the nonsmooth transition (at $\omega = 2$) is depicted and in (c) a bifurcation diagram for $1.5 < \omega < 2.5$. The different curves in (a) and (b) represent period-one (O - 'solid' and I - 'solid'), period-two (II - '--'), and period-three (III - '-· -') motion. See also Fig. 5, where the actual trajectories are depicted.

as κ increases this orbit goes through a series of transitions associated with corner events, leading to much more complex behaviour. In contrast to the $\kappa = 0$ case (in Fig. 4), where there was clearly **one** corner bifurcation present, there seem to be **two** corner bifurcations at points $\kappa = \kappa_C < \kappa_{CC} < 0$. The overall dynamics is much more complex with high-period orbits, and with many impacts per period occurring between relatively simple periodic motions. For $\kappa \approx 0$ the periodic solution has two impacts per period and for $\kappa \approx -0.015$ one impact. For instance, for $\kappa = -0.014$ a period-25 orbit appears as can be seen in Fig. 6.

We now proceed to give a brief description of the simple periodic motions and the conditions for these to have corner bifurcations. In secs. 4 and 5 we then look at the dynamics close to the corner bifurcation points.

3.3 Global behaviour of simple periodic orbits

In this section we will present a global analysis of the observed periodic orbits, concentrating on the existence of different types of orbit and establishing conditions for the occurrence of a corner event.

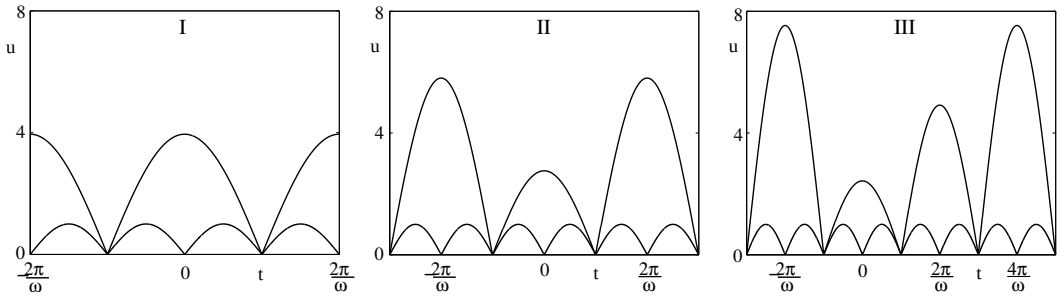

Figure 5: Time series at $\omega = 1.999$ of the three distinct types of periodic orbits created at $\omega_s = 2$, where I, II, and III show period-one, period-two, and period-three motion, respectively.

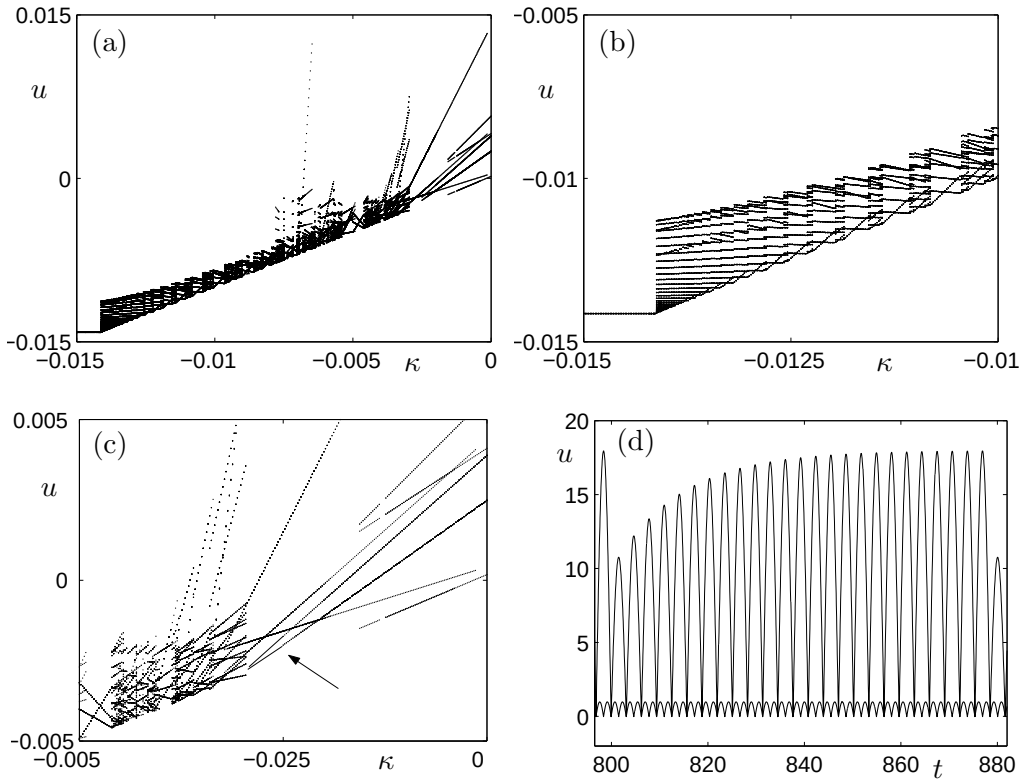

Figure 6: (a) A bifurcation diagram for $\omega = 1.999$ showing the position u at impact as κ is varied. (b) A blow-up of (a) in the vicinity of the corner bifurcation of the single impacting orbit. (c) A blow-up of (a) in the vicinity of the corner bifurcation of the orbit with two impacts (see the arrow). (d) Time history for $\kappa = -0.014$ and $\omega = 1.999$ (cf. (b)).

3.3.1 Single impact periodic orbits

We assume initially, that for a certain set of parameter values, the particle u has a periodic orbit with a single impact per period at a time (or times) τ close to a point t_k where z loses smoothness. We then consider the situation where, as a parameter varies, τ coincides with t_k so that a corner event occurs.

To study the behaviour of the periodic solutions bifurcation, we introduce a Poincaré surface Π at the time $t = nT = 2n\pi/\omega$ and consider a map induced by the flow so that

$$(a, b) = (u(0), v(0)) \to (u(T), v(T)) = (A, B).$$

Close to $t = 0$ (away from impact) we have $u(t) = a\cos(t) + b\sin(t)$ and close to $t = T$ we have $u(t) = A\cos(t - T) + B\sin(t - T)$.
We assume at present that there is a single impact orbit of period T for which the impact of u with z occurs at a point τ slightly after a (first) point t_0 with $0 < t_0 < T$ where z loses smoothness. The reasons for this choice of τ will become clear presently. Close to t_0 z behaves as (7), and in this case it follows that a, b and A, B are related as follows. The condition for an impact gives

$$a\cos(\tau) + b\sin(\tau) = A\cos(\tau - T) + B\sin(\tau - T) = \kappa + \theta_2(\tau - t_0)$$

and the change in the velocity at impact gives

$$-A\sin(\tau - T) + B\cos(\tau - T) = (1 + r)\theta_2 + ra\sin(\tau) - rb\cos(\tau),$$

where the impact law (5) is used. If a, b are known, then solving this system for A, B and τ gives a nonlinear map $P_S(a, b)$ to A, B and τ. A necessary condition for the existence of a single period periodic orbit is that $(a, b) = (A, B)$. If τ is given this leads to the following linear system for a, b and κ

$$\begin{pmatrix} \cos(\tau) & \sin(\tau) & -1 \\ \cos(\tau) - \cos(\tau - T) & \sin(\tau) - \sin(\tau - T) & 0 \\ -r\sin(\tau) - \sin(\tau - T) & r\cos(\tau) + \cos(\tau - T) & 0 \end{pmatrix} \begin{pmatrix} a \\ b \\ \kappa \end{pmatrix} = \begin{pmatrix} \theta_2(\tau - t_0) \\ 0 \\ (1 + r)\theta_2 \end{pmatrix},$$

the solution of which can be expressed as

$$(a, b, \kappa + \theta_2(\tau - t_0)) = \theta_2 \frac{(1 + r)}{(1 - r)} \left(\frac{\sin(\tau) - \sin(\tau - T)}{(1 - \cos(T))}, \frac{\cos(\tau - T) - \cos(\tau)}{(1 - \cos(T))}, \cot(T/2) \right). \tag{10}$$

Now consider the forcing $z(t) = \kappa + \beta|\sin(\omega t)|$. For this we have $t_0 = \pi/\omega$, $T = 2\pi/\omega$ and $\theta_1 = \theta_2 = \beta\omega$. A corner bifurcation then occurs when $\tau = t_0$. Substituting, this arise at parameter values (ω_C, κ_C) satisfying the condition

$$\omega_C \frac{(1 + r)}{(1 - r)} \cot(\pi/\omega_C) = \kappa_C. \tag{11}$$

At the bifurcation point we also have

$$a = \omega_C \frac{(1 + r)}{(1 - r)} \frac{1}{\sin(\pi/\omega_C)}, \quad \text{and} \quad b = 0. \tag{12}$$

For each fixed κ_C there is a locally unique value of ω_C so that we have a codimension-one condition for a corner bifurcation. If $\kappa_C = 0$ this occurs when $\omega_C = 2$ as we can observe from the bifurcation diagram in Fig. 4.

More generally, a single impact periodic orbit exists when

$$\kappa = \omega \frac{(1 + r)}{(1 - r)} \cot(\pi/\omega) + \theta_2(t_0 - \tau).$$

Thus, as $\tau > t_0$ the region of existence of the single impact orbit is given by

$$\kappa < \kappa_C \quad \text{or} \quad \omega > \omega_C, \tag{13}$$

and if ω is fixed the complex behaviour may (and indeed does) arise as κ increases through κ_C, or equivalently as ω decreases below ω_C.

3.3.2 Double-impact periodic orbits

We may repeat this analysis by looking at periodic orbits with *two* impacts, one just before t_0 and the other just after t_0. If the two impacts are close then we may approximate the flow between them by a straight line with constant velocity v, which considerably simplifies the analysis. If the impacts are at times $\tau^- < t_0$ and $\tau^+ > t_0$ then (using the notation of the previous subsection) a double-impact periodic orbit arises when we can solve the system

$$a\cos(\tau^-) + b\sin(\tau^-) = \kappa + \theta_1(t_0 - \tau^-),$$
$$a\cos(\tau^+ - T) + b\sin(\tau^+ - T) = \kappa + \theta_2(\tau^+ - t_0).$$

From the impact law we have

$$v + \theta_1 = -r(-a\sin(\tau^-) + b\cos(\tau^-) + \theta_1)$$

and

$$-r(v - \theta_2) = -a\sin(\tau^+ - T) + b\cos(\tau^+ - T) - \theta_2.$$

Finally, the assumption of constant velocity and small time of flight yields

$$\theta_1(t_0 - \tau^-) + v(\tau^+ - \tau^-) = \theta_2(\tau^+ - t_0).$$

From this we can now find τ^-- and τ^+-dependent expressions for the existence of periodic motions with two impacts, e.g.

$$\begin{aligned}\kappa &= \frac{(\theta_2 + r\theta_1)(1+r)}{1+r^2}\cot\left(\frac{T+\tau^- - \tau^+}{2}\right) + \dots \\ &\quad \frac{\theta_1\left(1 - r^2 c_{T+\tau^- - \tau^+}\right)(t_0 - \tau^-) + \theta_2\left(r^2 - c_{T+\tau^- - \tau^+}\right)(\tau^+ - t_0)}{(1+r^2)\left(1 - c_{T+\tau^- - \tau^+}\right)}, \quad (14)\end{aligned}$$

where $c_{T+\tau^- - \tau^+} = \cos(T + \tau^- - \tau^+)$. A corner event arises when both impacts (and thus τ^- and τ^+) approach $t_0 = T/2 = \pi/\omega$, which yields the following solution for a, b, and κ

$$(a, b, \kappa) = \frac{(\theta_2 + r\theta_1)(1+r)}{1+r^2}\left(\frac{-1}{\sin(\frac{\pi}{\omega})}, 0, \cot\left(\frac{\pi}{\omega}\right)\right). \quad (15)$$

The case of $u_0 = \kappa + |\sin(\omega t)|$ has $\theta_1 = \theta_2 = \omega$. This gives

$$(a, b, \kappa) = \omega\frac{(1+r)^2}{1+r^2}\left(\frac{1}{\sin\left(\frac{\pi}{\omega}\right)}, 0, \cot\left(\frac{\pi}{\omega}\right)\right), \quad (16)$$

so that a corner bifurcation occurs for the double impacting case when $(\omega, \kappa) = (\omega_{CC}, \kappa_{CC})$ satisfy the condition

$$\kappa_{CC} = \omega_{CC}\frac{(1+r)^2}{1+r^2}\cot\left(\frac{\pi}{\omega_{CC}}\right). \quad (17)$$

Following the methodology in sec. 3.3.1 and the analysis above we have that a double impact periodic orbit exists when

$$\begin{aligned}\kappa &= \omega\frac{(1+r)^2}{1+r^2}\cot\left(\frac{\pi}{\omega} + \frac{\tau^- - \tau^+}{2}\right) + \dots \\ &\quad \frac{\theta_1\left(1 - r^2 c_{\pi/\omega + \tau^- - \tau^+}\right)(t_0 - \tau^-) + \theta_2\left(r^2 - c_{\pi/\omega + \tau^- - \tau^+}\right)(\tau^+ - t_0)}{(1+r^2)\left(1 - c_{\pi/\omega + \tau^- - \tau^+}\right)}. \quad (18)\end{aligned}$$

Thus, as $\tau^- < t_0$ and $\tau^+ > t_0$ we can show that the region for the existence of a double impact orbit is given by

$$\kappa > \kappa_{CC} \quad \text{or} \quad \omega < \omega_{CC}. \tag{19}$$

3.3.3 The corner bifurcation

It is notable that the conditions (11) and (17) differ so that for the same value of κ the period-one motions with one and two impacts experience corner bifurcations at different frequencies ω, as seen in Fig. 7. However, it is also clear from the figure

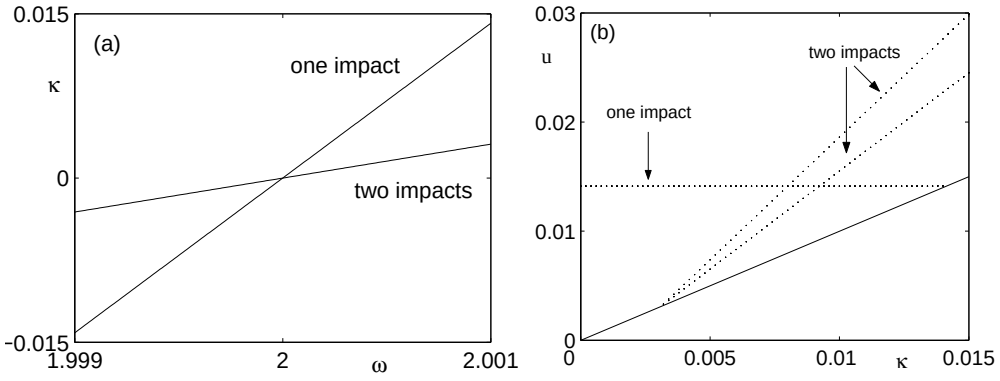

Figure 7: (a) The two curves given by the conditions (11) and (17) in a vicinity of $\omega = 0$. (b) A bifurcation diagram for $\omega = 2.001$ showing the impact height for period-one orbits with one and two impacts as κ is varied. The solid line shows the location of the corner point as a function of κ. When the branches of periodic orbits coincide with the solid line a corner bifurcation occurs. In both cases the coefficient of restitution $r = 0.8$.

that the point $(\omega, \kappa) = (2, 0)$ lies on the intersection of these two curves, and that they are linear close to this point. From the discussion above we can also conclude that period-one motion with one impacts is expected *below* one of the curves, so that $\omega > \omega_C$ or $\kappa < \kappa_C$ and period-one motion with *two* impacts is expected *above* the other curve so that $\omega < \omega_{CC}$ or $\kappa > \kappa_{CC}$ (see Fig. 7(a)).

This suggests that for

$$\omega > 2 \quad \text{and} \quad \kappa > 0$$

different period-one periodic orbits with one and two impacts should coexist over a range of values and that there is a possibility for hysteresis effects as ω is varied. In the right panel of Fig. 7 this situation has been captured for $\omega = 2.001$ and varying κ. The two bifurcation points, at $\kappa = 0.00157$ for the motion with two impacts per period and at $\kappa = 0.0141$ for the case with one impact, perfectly match what the analytic expressions (11) and (17) depicted in Fig. 7(a) predicts.

In contrast, if

$$\omega < 2 \quad \text{and} \quad \kappa < 0$$

there is a range of values of ω given by $\omega_{CC} < \omega < \omega_S$ (or equivalently $\kappa_C < \kappa < \kappa_{CC}$) for which neither period-one periodic motion with one impact nor two impacts can exist. The dynamics in this case is complex and the analysis of it

will be the subject of Sections 4 and 5. Possible dynamics could include period-N motion, for arbitrary $N > 1$, with a possible motion comprising $N-1$ impacts *after* the corner point followed by one *before* it. Other combinations of impact sequence are also possible. A numerical investigation of precisely this region was presented in Fig. 6(a), where $\omega = 1.999$ and $r = 0.8$ and κ is varies through the interval $[\kappa_C, \kappa_{CC}]$. The corner events are again predicted by the $\kappa - \omega$ plot in the left panel of Fig. 7 and it follows from (13) and (19) that in this case

$$\kappa_C = -0.014137 \quad \text{and} \quad \kappa_{CC} = -0.003103.$$

In Fig. 6(b) a blow up of the bifurcation diagram close to the corner bifurcation at $\kappa = \kappa_C$ for the period-one orbit with one impact is presented. At the bifurcation point we can clearly see a sudden jump from the simple periodic motion for $\kappa < \kappa_C$ to a sequence of different high periodic motions as κ is increased. Indeed, the bifurcation diagram displays a *period-adding* sequence with the period N of the orbit increasing in jumps of one as κ decreases to κ_C. A time history of one of the high-period orbits (a period-25 orbit) at $\kappa = -0.0140$ is shown in Fig. 6(d). Similarly, Fig. 6(c) shows a bifurcation diagram in a neighbourhood of the corner bifurcation at $\kappa = \kappa_{CC}$ for the period-one orbit with two impacts. From this analysis we can also suspect that there exists a large number (or an infinite number) of curves in the $\omega - \kappa$ plane, where each represent corner bifurcations for motions of different periodicity.

4 2D maps

4.1 The local form of the Poincaré map close to $(\omega, \kappa) = (2, 0)$.

The discussion at the end of the last section, and in particular the results presented in Fig. 7 indicate that we expect to see interesting dynamics for parameter values close to $\omega = 2$ and $\kappa = 0$. To understand this dynamics and the nature of the *corner bifurcation* we now present an analysis of the local form of the Poincaré map P given by $(A, B) = P(a, b)$ on the assumption that u has an impact or impacts with z very close to the corner point at $t_0 = \pi/\omega$ with $z(t) = \kappa + |\sin(\omega t)|$. To do this analysis we will assume that $|\kappa| = \mathcal{O}(\varepsilon)$, $|\omega - 2| = \mathcal{O}(\varepsilon)$ and $|\varepsilon| \ll 1$. We will show that for ε small, the map P, to leading order, takes three different linear forms, depending on (directly) on the location of the impact(s) and (indirectly) on the values of a and b. We identify three situations (see also Fig. 8):

case α - two impacts one just before and one just after t_0,

case β - an impact at a time τ just after t_0, and

case γ - an impact at a time τ just before t_0,

In the derivation of the three different maps we analyse the system (8) and (9), with

$$\omega = 2 + \omega_1 \varepsilon + \omega_2 \varepsilon^2 + \ldots, \tag{20}$$

$$\kappa = \kappa_1 \varepsilon + \kappa_2 \varepsilon^2 + \ldots. \tag{21}$$

We will also assume that (a, b) and (A, B) have asymptotic expansions of the form

$$a = a_0 + a_1 \varepsilon + a_2 \varepsilon^2 + \ldots, \quad b = b_0 + b_1 \varepsilon + b_2 \varepsilon^2 + \ldots, \tag{22}$$

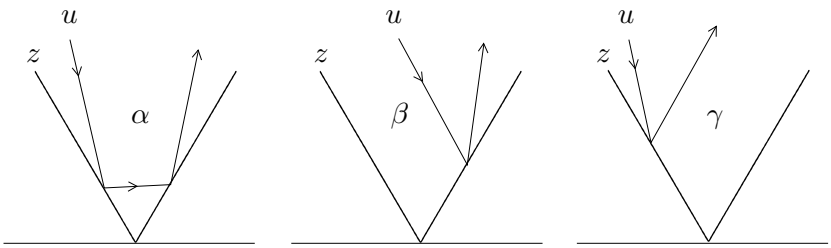

Figure 8: Schematics of the three orbits leading to the three local maps α, β and γ.

and

$$A = A_0 + A_1\varepsilon + A_2\varepsilon^2 + \ldots, \quad B = B_0 + B_1\varepsilon + B_2\varepsilon^2 + \ldots, \tag{23}$$

where we assume that $a_0, A_0 > 0$, so that the trajectory for u is initially above z.

4.2 The β-map

This is the simplest case to analyse and arises when there is a first impact just after $t_0 = \frac{\pi}{\omega}$ at a time

$$\tau = \frac{\pi}{\omega} + \tau_1\varepsilon + \tau_2\varepsilon^2 + \ldots. \tag{24}$$

Using (8) and (9) the relations for a single impact with u_2 at $t = \tau$ are given by

$$a\cos(\tau) + b\sin(\tau) = \kappa + |\sin(\omega\tau)| \tag{25}$$

and

$$A\cos(\tau - 2\pi/\omega) + B\sin(\tau - 2\pi/\omega) = \kappa + |\sin(\omega\tau)|\,. \tag{26}$$

Now, using (22) and (23) we can expand (25) and (26) about $\varepsilon = 0$, and look at terms in successive powers of ε.

To leading order we have

$$b_0 = -B_0 = 0.$$

To order ε we have

$$(2 + a_0)\tau_1 = \frac{\pi}{4}a_0\omega_1 + b_1 - \kappa_1 \tag{27}$$

and

$$(2 - A_0)\tau_1 = \frac{\pi}{4}A_0\omega_1 - B_1 - \kappa_1. \tag{28}$$

Eliminating τ_1 between (27) and (28) gives

$$(2 - A_0)(\pi a_0\omega_1/4 + b_1 - \kappa_1) = (2 + a_0)(\pi A_0\omega_1/4 - B_1 - \kappa_1). \tag{29}$$

Now, suppose that the velocity just before impact is v^- and just after is v^+ so that

$$v^- = -a\sin(\tau) + b\cos(\tau) \quad \text{and} \quad v^+ = -A\sin(\tau - 2\pi/\omega) + B\cos(\tau - 2\pi/\omega). \tag{30}$$

Expanding the expressions (29) and (30) and substituting $b_0 = B_0 = 0$ gives

$$v^- = -a_0 - a_1\varepsilon + \mathcal{O}\left(\varepsilon^2\right), \quad v^+ = A_0 + A_1\varepsilon + \mathcal{O}\left(\varepsilon^2\right). \tag{31}$$

Now, from the impact law (5), we have to leading order that

$$v^+ = (1 + r)\theta_2 - rv^- = 2(1 + r) - rv^-. \tag{32}$$

Substituting (31) into (32) we have to leading order

$$A_0 = 2(1+r) + ra_0 \quad \text{so that} \quad (A_0 - 2) = r(a_0 + 2). \tag{33}$$

If we substitute (32) into (29) we have

$$\begin{aligned} A_0 &= ra_0 + 2(1+r), & (34)\\ B_1 &= \frac{\pi\omega_1 r}{2} a_0 + rb_1 + (1+r)\left(\frac{\pi\omega_1}{2} - \kappa_1\right). & (35) \end{aligned}$$

The above linear two-dimensional map captures the dynamics of the β-map to order ε. Note that A_0 is a function of a_0 alone.

In order to apply the β-map it is necessary to determine whether the impact does indeed occur after the time $t_0 = \pi/\omega$ so that $\tau > \pi/\omega$. To order ε this implies that $\tau_1 > 0$. Thus from (27), and the assumption that $a_0 > 0$ it follows that the Poincaré map is a β-map if the following linear compatability condition is satisfied

$$\frac{\pi}{4} a_0\omega_1 + b_1 - \kappa_1 > 0. \tag{36}$$

4.3 The γ-map

The derivation of the γ-map is very similar to that of the β-map, i.e. eqs. (25) and (26) must hold and we do the perturbations (20) and (24) and the ansätze (22) and (23). After expanding (25) and (26) we get $b_0 = B_0 = 0$ and

$$\begin{aligned} A_0 &= ra_0 - 2(1+r), & (37)\\ B_1 &= \frac{\pi\omega_1 r}{2} a_0 + rb_1 - (1+r)\left(\frac{\pi\omega_1}{2} + \kappa_1\right). & (38) \end{aligned}$$

Since the γ-map (35) can only be applied if the impact time $\tau < \pi/\omega$, we know that $\tau_1 < 0$ and thus from (27) the γ-map applies if

$$\frac{\pi}{4} a_0\omega_1 + b_1 - \kappa_1 < 0. \tag{39}$$

As the function u is locally convex, a sufficient condition guaranteeing that there is no further impact close to τ is that $v^+ > \theta_2$. This gives the further condition

$$v^+ = (1+r)\theta_1 - rv^- > \theta_1 \quad \Longrightarrow \quad v^- < \theta_2 + \frac{\theta_2 - \theta_1}{r} = -2 - \frac{4}{r}. \tag{40}$$

To leading order this is satisfied provided that

$$a_0 > 2 + \frac{4}{r}. \tag{41}$$

The condition (41) then determines whether we can apply the $\gamma-$map rather than the $\alpha-$map.

4.4 The α-map

The main difference between the γ- and α-maps is that the γ-map involves one impact just before t_0 and the α-map two impacts, one before and one after t_0. We assume that these occur at the times

$$\tau^- = \pi/\omega - \varepsilon\delta_1 + \mathcal{O}(\varepsilon^2) \quad \text{and} \quad \tau^+ = \pi/\omega + \varepsilon\delta_2 + \mathcal{O}(\varepsilon^2).$$

To derive the α-map we first notice that

$$\begin{aligned} a\cos(\pi/\omega - \varepsilon\delta_1) + b\sin(\pi/\omega - \varepsilon\delta_1) &= \kappa + |\sin(\pi - \omega\varepsilon\delta_1)|\,, \quad (42)\\ A\cos(-\pi/\omega + \varepsilon\delta_2) + B\sin(-\pi/\omega + \varepsilon\delta_2) &= \kappa + |\sin(-\pi + \omega\varepsilon\delta_2)|\,, \quad (43)\end{aligned}$$

Expanding to order ε gives

$$\begin{aligned} \frac{\pi}{4}a_0\omega_1 - a_0\delta_1 + b_1 &= \kappa_1 + 2\delta_1, \quad (44)\\ \frac{\pi}{4}A_0\omega_1 + A_0\delta_2 - B_1 &= \kappa_1 + 2\delta_2. \quad (45)\end{aligned}$$

The time interval between the nearby impacts is $\varepsilon(\delta_1+\delta_2)$ and the velocity immediately after the first impact is (to leading order) $v^+ = -2(1+r)+ra_0$. The trajectory between the two impacts is linear to order ε giving

$$\kappa_1 + 2\delta_1 + (\delta_1+\delta_2)(ra_0 - 2(1+r)) = \kappa_1 + 2\delta_2. \quad (46)$$

From (44)-(46) we get the linear system

$$\begin{pmatrix} -a_0 - 2 & 0 & 0 \\ 0 & A_0 - 2 & -1 \\ r - \frac{1}{2}ra_0 & r + 2 - \frac{1}{2}ra_0 & 0 \end{pmatrix} \begin{pmatrix} \delta_1 \\ \delta_2 \\ B_1 \end{pmatrix} = \begin{pmatrix} -b_1 + \kappa_1 - \frac{\pi}{4}a_0\omega_1 \\ \kappa_1 - \frac{\pi}{4}a_0\omega_1 \\ 0 \end{pmatrix} \quad (47)$$

with solution

$$\begin{aligned} \delta_1 &= \frac{b_1 - \kappa_1 + \frac{\pi}{4}a_0\omega_1}{a_0 + 2}, \quad (48)\\ \delta_2 &= \frac{r(a_0-2)\left(\kappa_1 - b_1 - \frac{\pi}{4}a_0\omega_1\right)}{(a_0+2)(r(a_0-2)-4)}, \quad (49)\\ B_1 &= \frac{r(A_0-2)(a_0-2)\left(\kappa_1 - b_1 - \frac{\pi}{4}a_0\omega_1\right)}{(a_0+2)(r(a_0-2)-4)} - \kappa_1 + \frac{\pi}{4}a_0\omega_1. \quad (50)\end{aligned}$$

In the same fashion as for the β- and γ-maps, if we let v^- be the impact velocity of u at the first impact and v^+ the velocity just after the second impact, and assuming that the velocity after the first impact is equal to the impact velocity at the second impact, the impact law (5) gives to leading order that

$$\begin{aligned} v^+ &= (1+r)\theta_1 - r\left((1+r)\theta_2 - rv^-\right) = 2(1+r)^2 + r^2v^-, \quad \Longleftrightarrow\\ A_0 &= 2(1+r)^2 - r^2a_0. \quad (51)\end{aligned}$$

Substituting (51) into (50) gives the full two-dimensional α-map

$$\begin{aligned} A_0 &= -r^2a_0 + 2(1+r)^2, \quad (52)\\ B_1 &= \frac{-r^2\pi\omega_1}{2}a_0 - r^2b_1 + \frac{\pi\omega_1}{2}(1+r)^2 + \kappa_1(r^2-1). \quad (53)\end{aligned}$$

Now we know from the analysis of the γ-map that to have an impact prior to the corner event we must have

$$\frac{\pi}{4}a_0\omega_1 + b_1 - \kappa_1 < 0. \quad (54)$$

To also have an impact just after the corner event we have from (55) that

$$a_0 < 2 + \frac{4}{r}. \quad (55)$$

4.5 Transitions

The map P is thus, to leading order, piece-wise linear and is discontinuous across three lines, the location of which depends upon κ_1 and ω_1. We denote the three regions where each map applies as S_α, S_β and S_γ. These regions are illustrated in Fig. 9. The boundary Σ_β between S_β and either S_α or S_γ is given by

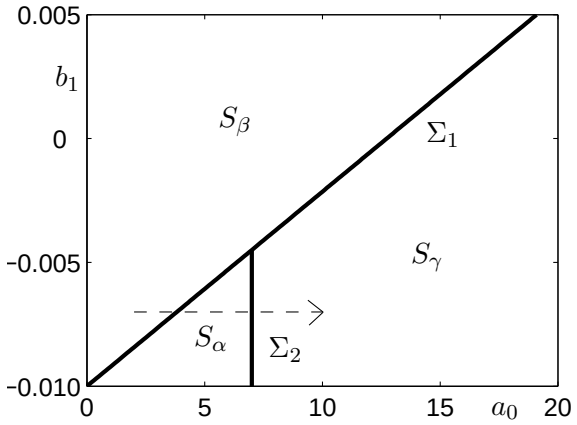

Figure 9: The regions S_α, S_β and S_γ and boundaries Σ_α, Σ_β for $\omega = 1.999$ and $\kappa = -0.01$.

$$\Sigma_1 = \{(a_0, b_1) : \pi\omega_1 a_0/4 + b_1 - \kappa_1 = 0\},$$

and that between S_α and S_γ by

$$\Sigma_2 = \{(a_0, b_1) : a_0 - 2 - 4/r = 0,\ \pi\omega_1 a_0/4 + b_1 - \kappa_1 \leq 0\}.$$

The transition as we cross Σ_1 is a *corner event* with an impact occurring at t_0. In contrast, the transition as we cross Σ_2 is a *grazing event* [12, 28, 29, 17], involving a grazing impact between z and u close to t_0. A more refined analysis (see for example [26]) of the grazing event shows that this has a square-root form. The discontinuous map is an outer approximation to this. We illustrate this in Fig. 10 by taking $\omega = 1.999, \kappa = -0.01, b = -0.007$ and varying a_0 from 2 to 10 (as illustrated with the arrow in Fig. 9). This set of initial data involves an initial transition from S_β to S_α and then to S_γ. We plot A_0 as a function of a_0 and compare this (Fig. 10(a)) with the linear form (Fig. 10(b)) of the three maps.

The change in the stability of a fixed point as it crosses a grazing line is well understood [12, 26, 28] and we do not discuss it further here. Of interest is the case of the corner bifurcation which arises when a fixed point crosses the line Σ_1.

5 The dynamics of the linearised system close to a corner bifurcation

From the analysis presented in sec. 4 it follows that if ω is close to 2 and κ is close to zero then the local dynamics close to a corner event can be described by one of three linear two-dimensional maps and their associated compatability conditions. If

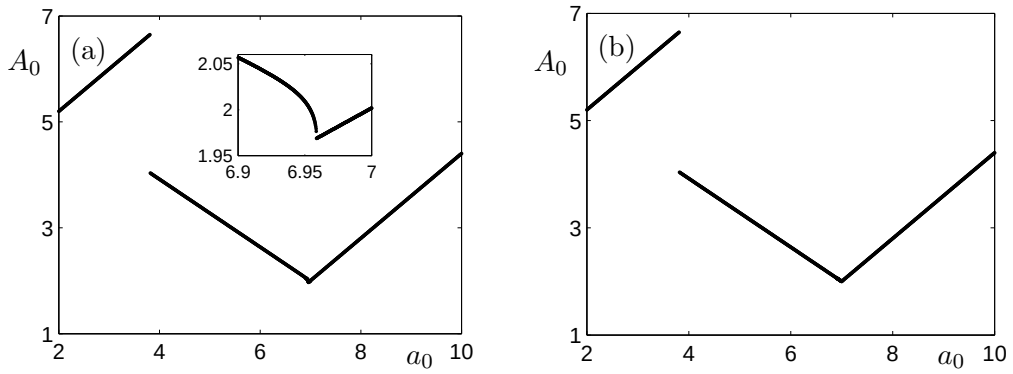

Figure 10: (a) The original impacting system. The inset shows the local form close to the corner bifurcation. (b) The linear form of the map.

we let $x = \begin{pmatrix} a_0 & b_1 \end{pmatrix}^T$ the three maps α, β and γ act on the two-dimensional vector x to generate a series of iterations in the manner

$$x_{n+1} = P(x_n) = \begin{cases} Q_\alpha x_n + P_\alpha & \text{if } Cx_n < \kappa_1 \text{ and } Dx_n < E, \\ Q_\beta x_n + P_\beta & \text{if } Cx_n > \kappa_1, \\ Q_\gamma x_n + P_\gamma & \text{if } Cx_n < \kappa_1, \text{ and } Dx_n > E, \end{cases} \tag{56}$$

where

$$Q_\alpha = -r^2 \begin{pmatrix} 1 & 0 \\ \frac{\pi\omega_1}{2} & 1 \end{pmatrix}, \quad Q_\beta = Q_\gamma = r \begin{pmatrix} 1 & 0 \\ \frac{\pi\omega_1}{2} & 1 \end{pmatrix}, \tag{57}$$

$$P_\alpha = \begin{pmatrix} 2(1+r^2) \\ \frac{r\pi\omega_1}{2}(1+r^2) + \kappa_1(r^2-1) \end{pmatrix}, \tag{58}$$

$$P_\beta = (1+r) \begin{pmatrix} 2 \\ \frac{\pi\omega_1}{2} - \kappa_1 \end{pmatrix}, \quad P_\gamma = -(1+r) \begin{pmatrix} 2 \\ \frac{\pi\omega_1}{2} + \kappa_1 \end{pmatrix}, \tag{59}$$

$$C = \begin{pmatrix} \frac{\pi\omega_1}{4} & 1 \end{pmatrix}, \; D = \begin{pmatrix} 1 & 0 \end{pmatrix} \text{ and } E = 2 + \frac{4}{r}. \tag{60}$$

The dynamics of the impacting system close to the corner event can thus be analysed in terms of the dynamics of a piece-wise linear, discontinuous, two-dimensional map. The similar situation of the analysis of a discontinuous one-dimensional map has been considered by various authors [24, 6, 20, 21] with some recent computations given in [23]. All observe period-adding cascades in the one dimensional system for certain ranges of parameters, similar to those we see in Fig. 6(b). We now give a similar analysis for the two-dimensional case by looking at fixed points, periodic orbits and period adding for the maps in (56). Typical observed dynamics is a sequence of iterations of one map (say β) followed by iterations of another (say γ) combining to give more complex dynamics.

5.1 Fixed points

The simplest form of the dynamics is a fixed point of each of the three maps taken individually. These correspond to periodic orbits of the flow as constructed in section 3, so that a fixed point of the $\beta-$map is a single impact periodic orbit, and that of

the $\alpha-$map is a double impact periodic orbit. If we consider, at present, that each map acts over the whole of the plane, then these fixed points (56) are given by

$$x^*_\cdot = (I - Q_\cdot)^{-1} P_\cdot, \tag{61}$$

where $x^*_\cdot = \begin{pmatrix} a^*_\cdot & b^*_\cdot \end{pmatrix}^T$. Setting

$$\kappa_\cdot = \frac{\pi\omega_1 a^*_\cdot}{4} \tag{62}$$

the fixed points are given by

$$x^*_\alpha = \begin{pmatrix} \frac{2(1+r)^2}{1+r^2} & \frac{1-r^2}{1+r^2}(\kappa_\alpha - \kappa_1) \end{pmatrix}^T, \tag{63}$$

$$x^*_\beta = \begin{pmatrix} \frac{2(1+r)}{1-r} & \frac{1+r}{1-r}(\kappa_\beta - \kappa_1) \end{pmatrix}^T, \tag{64}$$

$$x^*_\gamma = \begin{pmatrix} -\frac{2(1+r)}{1-r} & \frac{1+r}{1-r}(\kappa_\gamma - \kappa_1) \end{pmatrix}^T. \tag{65}$$

The dynamics of the different maps close to the fixed points can now be written simply as

$$x_n = x^*_\cdot + Q^n_\cdot (x_0 - x^*_\cdot), \tag{66}$$

where

$$Q^n_\alpha = (-r^2)^n \begin{pmatrix} 1 & 0 \\ \frac{n\pi\omega_1}{2} & 1 \end{pmatrix}, \quad Q^n_\beta = Q^n_\gamma = r^n \begin{pmatrix} 1 & 0 \\ \frac{n\pi\omega_1}{2} & 1 \end{pmatrix}. \tag{67}$$

As $0 < r < 1$ each fixed point is stable. Observe that each point is a *degenerate node* with all iterates in the appropriate domain of definition asymptotically approaching $x^*_\cdot$ along the vector $\begin{pmatrix} 0 & 1 \end{pmatrix}^T$.
In each case the fixed point may or may not satisfy the compatability conditions associated with its map. If it satisfies the compatability condition then, as it is stable, it will be observed as the limit of iterates in the appropriate domain of definition. (Of course other fixed points may exist in other regions). If it does not, then it will not be observed directly, but may strongly influence the dynamics. For example the fixed point x^*_β may lie in S_γ but may attract iterates of the map β in S_β. Typical dynamics will then comprise a series of iterates in S_β moving towards x^*_β followed by iterates of γ.

A corner bifurcation of the form observed in sec. 3, typically arises when, as parameters vary, a fixed point of one of the maps moves to intersect the set Σ_1 determining the first compatability condition $Cx - \kappa_1 = 0$. We now study the conditions under which this will happen.

5.2 The compatability conditions

The condition for the existence of the fixed point of the $\beta-$map is given by

$$c_\beta \equiv \pi\omega_1 a^*_\beta/4 + b^*_\beta - \kappa_1 > 0.$$

After some manipulation (and using (64)) we have

$$c_\beta = \frac{2}{1-r}(\kappa_\beta - \kappa_1).$$

Thus we see a transition when $\kappa_\beta = \kappa_1$ or equivalently when

$$\frac{\pi\omega_1}{2}\frac{(1+r)}{(1-r)} = \kappa_1,$$

and the existence of a fixed point of the β map when $c_\beta > 0$ so that

$$\kappa_1 < \frac{\pi\omega_1}{2}\frac{(1+r)}{(1-r)}. \tag{68}$$

This is precisely the linearisation of the condition (13).

Now consider the fixed point of the $\alpha-$map. The first condition for the existence is given by

$$c_\alpha \equiv \pi\omega_1 a^*_\alpha/4 + b^*_\alpha - \kappa_1,$$

so that, after some manipulation (and using (63))

$$c_\alpha = \frac{2}{1+r^2}(\kappa_\alpha - \kappa_1).$$

Thus x^*_α exists when $c_\alpha < 0$, so that $\kappa_\alpha < \kappa_1$ or

$$\frac{\pi\omega_1}{2}\frac{(1+r)^2}{(1+r^2)} < \kappa_1, \tag{69}$$

which is a linearisation of the condition (19).
We also require that $Dx < E$ so that $a^* < 2 + 4/r$. This is equivalent to the condition that

$$\frac{2(1+r)^2}{1+r^2} < 2 + \frac{4}{r}$$

which is satisfied for all r.

Finally consider the $\gamma-$map. In this case $a^* = -2(1+r)/(1-r) < 0$ so that this fixed point can never exist.

5.3 Simple periodic motion

5.3.1 Fixed points

As noted in Section 3, the (ω, κ) parameter space is divided into four regions determined by the existence/non-existence of the simple periodic orbits, and hence of the fixed points of the α and the β maps. If we set $\theta_\beta = \pi(1+r)/2(1-r)$ and $\theta_\alpha = \pi(1+r)^2/2(1+r^2)$ we see a $\beta-$fixed point if $\kappa_1 < \theta_\beta\omega_1$ and an $\alpha-$fixed point if $\kappa_1 > \theta_\alpha\omega_1$. As we move through parameter space we expect to see transitions between the various fixed points. In the simplest cases one fixed point disappears and is replaced by another and the resulting dynamics is relatively simple. An example of this arises when $\kappa_1 = 0$ and ω_1 varies through zero. If $\omega_1 > 0$ the $\beta-$fixed point is observed and is stable, whereas if $\omega_1 < 0$ the $\alpha-$fixed point is observed and is stable. We therefore expect to see a sudden jump from the $\beta-$fixed point to the $\alpha-$fixed point as ω_1 decreases through zero.

5.3.2 Low-period cycles

Whilst the $\alpha-$map is linear, and the fixed point x^*_α is stable, it is not a global attractor of the Poincaré map P and we do not only see the dynamics associated with the $\alpha-$fixed point. Indeed it is also very likely that periodic cycles will be observed involving a combination of two or more of the maps. Notationally we can describe such a cycle in terms of the symbol sequence of maps acting, so that a fixed point of the $\alpha-$map is denoted by (α) etc. When $\omega_1 < 0$ and $\kappa_1 = 0$ we also observe a two-cycle of the form $(\alpha\beta)$ and a three-cycle of the form $(\alpha\beta\gamma)$. These three periodic orbits can all be seen in Fig. 5.

These orbits are sequences satisfying the appropriate compatability condition. For example a necessary condition for the existence of the $(\alpha\beta)$ two cycle is that the solution of the identity

$$x = Q_\beta[Q_\alpha x + P_\alpha] + P_\beta$$

satisfies the two conditions

$$Cx - \kappa_1 < 0, \quad \text{and} \quad C[Q_\alpha x + P_\alpha] - \kappa_1 > 0.$$

This condition naturally generalises to more complex cycles.
In general, verifying the compatability conditions is difficult, however, calculating the values of a is simplified by the fact that the iteration on a does not involve b. Thus the value of a for the $(\alpha\beta)$ two-cycle follows from the identity

$$a = 2(1 + r) + r(2(1 + r^2) - r^2 a),$$

so that

$$a = \frac{2(1 + 2r + r^3)}{1 + r^3}.$$

The resulting $(\alpha\beta)$ two-cycle has a-values given by

$$\left(\frac{2(1 + 2r + r^3)}{1 + r^3}, \frac{2(1 - r^3)}{1 + r^3} \right).$$

It is easy (though tedious) to verify that this cycle satisfies the compatability conditions provided that $\omega_1 < 0$. Similarly, we can show that an $(\alpha\beta\gamma)$ three-cycle has values of a given by

$$\left(\frac{2(-1 + 2r^2 + r^4)}{(1 + r^4)}, \frac{2(1 + 2r^2 - r^4)}{(1 + r^4)}, \frac{2(1 + 2r + 2r^3 + r^4)}{(1 + r^4)} \right)$$

The three cycles (α), $(\alpha\beta)$ and $(\alpha\beta\gamma)$ appear from numerical experiments to be the only physical examples of periodic orbits when $\kappa_1 = 0$ and $\omega_1 < 0$ is small in modulus. A general theory for the existence of such periodic orbits would seem difficult to determine. See [29] for a study of periodic orbits in a quadratic system with two maps.

5.4 High-period periodic motion

The most interesting transitions arise when a parameter moves from a region where a single fixed point exists to one where no such point exists so that $\theta_\beta\omega_1 < \kappa_1 < \theta_\gamma\omega_1$. For example, if $\omega_1 < 0$ and κ_1 is increased from $-\infty$ to ∞ the β fixed point vanishes

when $\kappa_1 = \theta_\beta\omega_1$ and the motion has high period, periodic orbits. We give an example of orbits of the form $(\beta^N\gamma)$ where N approaches ∞ as κ_1 decreases to $\theta_\beta\omega_1$. Similarly, high period orbits of the form $(\alpha^N\beta)$ occur as κ_1 increases to $\theta_\alpha\omega_1$ to be replaced by the α fixed point if $\kappa_1 > \theta_\alpha\omega_1$.

To analyse this situation, we consider the case of κ_1 close to $\theta_\beta\omega_1$ and the dynamics of the β-map. With a slight abuse of earlier notation we set $x_n = (a_n, b_n)$ and initially assume that $x_0 = (a_0, b_0) \in S_\beta$ is given. Thus, while the β-map acts we have

$$\begin{pmatrix} a_n \\ b_n \end{pmatrix} = \begin{pmatrix} a^*_\beta \\ b^*_\beta \end{pmatrix} + r^n \begin{pmatrix} 1 & 0 \\ \frac{n\pi\omega_1}{2} & 1 \end{pmatrix} \begin{pmatrix} a_0 - a^*_\beta \\ b_0 - b^*_\beta \end{pmatrix}.$$

Now, consider the evolution of the variable $c_n = Cx_n - \kappa_1$ which measures the distance to the compatability set. Using the compatability conditions (36) and (39), and the above dynamics we can write

$$\begin{aligned} c_n &= \frac{\pi\omega_1 a_n}{4} + b_n - \kappa_1 \\ &= \frac{\pi\omega_1}{2}\frac{1+r}{1-r} + r^n\frac{\pi\omega_1}{4}(a_0 - a^*_\beta) - \kappa_1 + \frac{1+r}{1-r}(\kappa_\beta - \kappa_1) + \dots \\ &\quad nr^n\frac{\pi\omega_1}{2}(a_0 - a^*_\beta) + r^n(b_0 - b^*_\beta) \\ &= c_\beta + r^n\frac{\pi\omega_1}{4}(a_0 - a^*_\beta) + nr^n\frac{\pi\omega_1}{2}(a_0 - a^*_\beta) + r^n(b_0 - b^*_\beta). \end{aligned} \tag{70}$$

From (70) we see that if $c_\beta = \kappa_\beta - \kappa_1 > 0$ then as $n \to \infty$ we will always lie above the compatability line ($c_n > 0$) and therefore only have β dynamics.
On the other hand if $c_\beta < 0$ then, if $c_0 > 0$ there will be a first value N of n for which the compatability condition for the β-map is violated, so that $c_N \le 0$ and $c_{N-1} > 0$. We may then either have $x_N = (a_N, b_N) \in S_\alpha$ on in S_γ. Using (70) for large N we can estimate this first value from the identity

$$r^N N\frac{\pi\omega_1}{2}(a_0 - a^*_\beta) = \frac{2}{1-r}(\kappa_1 - \kappa_\beta). \tag{71}$$

Observe that $N \to \infty$ as $\kappa_1 - \kappa_\beta \to 0$.

We now consider the case of N large and set

$$\kappa_1 - \kappa_\beta = \delta \quad \text{with} \quad 0 < \delta \ll 1.$$

When the compatability condition (36) is first violated the next iterate of the map P will be either the α-map or the γ-map. As the iterations for large N lie asymptotically along the vector $\begin{pmatrix} 0 & 1 \end{pmatrix}^T$, the value of a_N will be very close to a^*_β. The γ-map is applied to x_N if $a^*_\beta > 2 + 4/r$ so that

$$\frac{2(1+r)}{1-r} > 2 + \frac{4}{r} \quad \text{or} \quad r^2 + r > 1$$

giving γ-dynamics if

$$r > \phi = 0.61803....$$

If $r < \phi$ then we apply the α-map to x_N.

Consider firstly the case of $r > \phi$. The fixed point x^*_β is mapped by γ to the point

$$x^{**}_\gamma = Q_\gamma x^*_\beta + P_\gamma$$

so that

$$a^{**} = \frac{2(1+r)(2r-1)}{(1-r)} \quad \text{and} \quad b^{**} = -\pi\omega_1(1+r).$$

If we calculate the compatability condition $Cx_\gamma^{**} - \kappa$ at the bifurcation point $\kappa = \kappa_\beta$ we have

$$c = \frac{\pi\omega_1 a^{**}}{4} + b^{**} - \kappa_\beta = \frac{\pi\omega_1}{2}\frac{(1+r)}{(1-r)}(r^2 + r - 2)$$

so that (as $r < 1$) $c > 0$ provided that $\omega_1 < 0$. It follows that $x_\gamma^{**} \in S_\beta$ provided that κ is close to κ_β.

Now consider the case of $r < \phi$ so that we apply the α map with the fixed point x_β^* mapped to the point

$$x_\alpha^{**} = Q_\alpha x_\beta^* + P_\alpha.$$

We now have

$$a^{**} = \frac{2(1-r-2r^3)}{(1-r)} \quad \text{and} \quad b^{**} = \frac{-\pi\omega_1(2r^2+r^4+1)}{2(1-r)}.$$

Thus, in this case, if $\kappa_1 = \kappa_\beta$

$$c = -\frac{\omega_1\pi}{(1-r)}(1+2r+2r^2+r^4),$$

so that $x_\alpha^{**} \in S_\beta$ if κ_1 is close to κ_β and δ is small.

5.4.1 Homoclinic orbits

If $\delta = 0^+$ we observe discontinuous homoclinic orbits that have the form $(\beta^\infty\gamma)$ if $r > \phi$ and $(\beta^\infty\alpha)$ if $r < \phi$. These arise as follows. The point x_β^* lies on the compatability set. As $\delta = 0^+$ this point is mapped to x^{**} by either the $\gamma-$map if $r > \phi$ or the α map if $r < \phi$. Following $N = \infty$ iterations of the $\beta-$ map we see a sequence in S_β tending towards x^* parallel to the vector $\begin{pmatrix} 0 & 1 \end{pmatrix}^T$. The two homoclinic orbits are illustrated in Fig. 11.

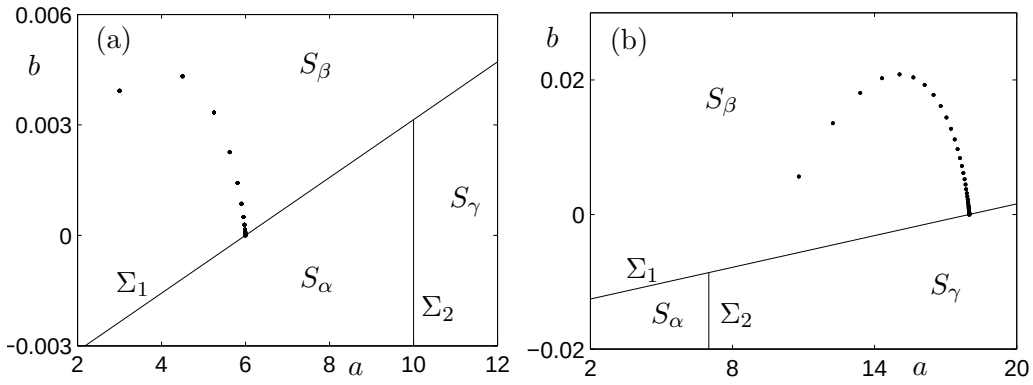

Figure 11: Homoclinic orbits with cycles (a) $(\beta^\infty\alpha)$ and (b) $(\beta^\infty\gamma)$, where $r = 0.5$ and $r = 0.8$, respectively.

5.4.2 High period orbits and period adding

More generally, if $0 < \delta \ll 1$ and $r > \phi$ we see a high period, periodic orbit of the form $(\beta^N\gamma)$, $N \gg 1$ which is a perturbation of the above homoclinic orbit. Similarly we see a $(\beta^N\alpha)$ orbit if $r < \phi$. For clarity we consider the $\beta^N\gamma$ orbit when $r > \phi$.

To construct this orbit, consider the case of $0 < \delta \ll 1$, so that the fixed point $x^*_\beta = \begin{pmatrix} 2(1+r)/(1-r) & -\delta(1+r)/(1-r) \end{pmatrix}^T$ lies just below the compatability set. Iterates of the $\beta-$map approach x^*_β along the line $x^*_\beta + \lambda \begin{pmatrix} 0 & 1 \end{pmatrix}^T$, for $\lambda > 0$. This line intersects the compatability set at the point

$$(a_c, b_c) = (a^*_\beta, \delta).$$

After some manipulation we find that the image of the point (a_c, b_c) under the action of the $\beta-$map is given by

$$\beta(a_c, b_c) = (a^*_\beta, -\delta).$$

The length 2δ interval

$$T = \{a = a^*_\beta, -\delta < b < \delta\} \subset S_\gamma$$

(which is close to $x^*_\beta \in S_\gamma$) is mapped into the region S_β and the resulting points are then attracted to x_β along the vector $\begin{pmatrix} 0 & 1 \end{pmatrix}^T$ eventually reentering T. The set T is thus a trapping region for the flow and we may identify a one-dimensional discontinuous map F from T to itself. We illustrate this set in Fig. 12.

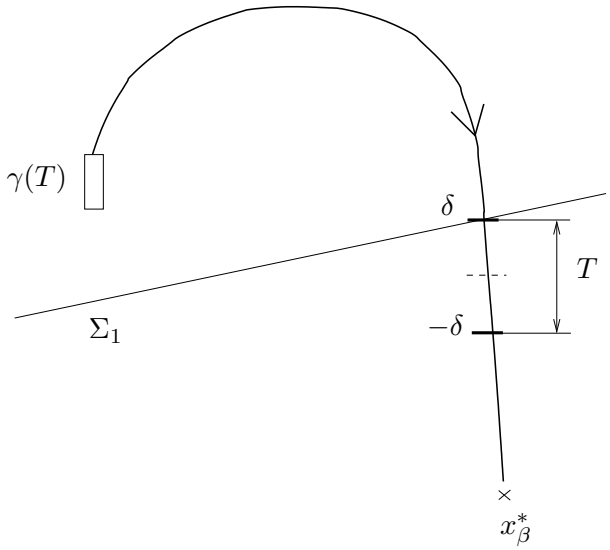

Figure 12: A schematic showing the mechanism behind the dynamics close to corner bifurcations.

The interval $T \subset S_\gamma$ is mapped by the $\gamma-$map to an interval $\gamma(T) \subset S_\beta$ of length $2r\delta$ close to the point $x^{**} \in S_\beta$. This interval will now be acted on by the $\beta-$map and the iterates $\beta^k\gamma(T)$ of the interval will initially lie in S_β. However, there will be a first value of $k = N$ when all or part of the set $\beta^N\gamma(T)$ lies inside $T \subset S_\gamma$. In the case of part of the set lying in T it follows, by construction that the points in $\beta^N\gamma(T)$ which do not lie in T will be mapped to points in the disjoint interval

$\beta^{N+1}\gamma(T)$ which do lie in T. This gives an implied (possibly discontinuous) map F from T to itself with $F = \beta^N\gamma$ or $\beta^{N+1}\gamma$. Note that F is a *piecewise linear* map with gradient r^{N+1} or r^{N+2}. We illustrate in Fig. 13 two cases of this function depending upon whether $\beta^N\gamma(T)$ lies wholly or partly in T.

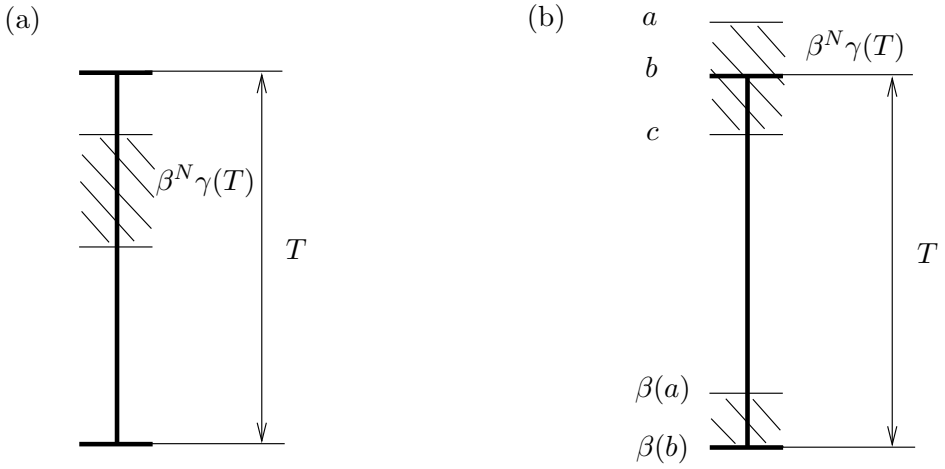

Figure 13: A schematic showing the mechanism behind the birth of intervals of high-periodic orbits.

Such maps resemble *circle maps* and have been studied by [24] and [6]. The analysis presented in these papers predicts that as $\delta \to 0^+$ we expect to see a sequence of high-period periodic orbits. If the *winding number* $W(\kappa)$ of these orbits is defined by the mean number of iterations in S_γ as a proportion of the total number of iterations, then the analysis in [6] predicts that $W(\kappa)$ is independent of the starting point in T, and that W is a continuous, monotone increasing function of κ which takes the form of a Cantor function which is locally constant over intervals of non-zero length (see also [33, 34]). We illustrate this in Fig. 14 for the case of $\omega = 1.999$ so that $\varepsilon\omega_1 = -0.001$ and $r = 0.8$ by plotting $W(\kappa)$ over a range of values of κ. We will show presently that for κ close to κ_C we have

$$W(\kappa) \sim 1/|\log(\kappa_1 - \kappa_\beta)|.$$

Without wishing to repeat this analysis in detail, we now give a simple explanation of this result by using the leading order approximation of the form of the maps when N is large. Suppose that we have a $(\beta^N\gamma)$ periodic orbit corresponding to a fixed point of F lying in T For large N we have (asymptotically to leading order)

$$b_N = \frac{Nr^N\pi\omega_1}{2}(a_0 - a^*_\beta) + b^*_\beta.$$

Then, applying the γ-map

$$(a_0, b_0) = \gamma(a^*_\beta, b_N) = (ra^*_\beta - 2(1+r), b_0).$$

Asymptotically this implies that

$$b_N = \frac{Nr^N\pi\omega_1}{2}((r-1)a^*_\beta - 2(1+r)) + b^*_\beta = \frac{-2Nr^N\pi\omega_1(1+r)}{2} - \frac{1+r}{1-r}\delta.$$

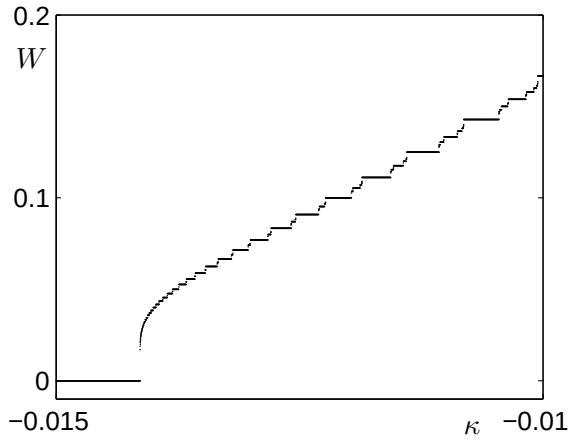

Figure 14: The function W showing the Cantor function form.

As we are only considering the case of $\omega_1 < 0$ there is a unique value of $N(\delta)$ such that $b_N \in T$ for which

$$\frac{-2Nr^N\pi\omega_1(1+r)}{2} - \frac{1+r}{1-r}\delta \in [-\delta, \delta].$$

The value of N is a piecewise constant function of δ. As the function Nr^N is monotone decreasing for large N, it follows that N is constant over the interval of δ values $\delta \in I_N \equiv (\delta_{N+1}, \delta_N)$ where

$$-2Nr^N\pi\omega_1(1+r) = \frac{1+r}{1-r}\delta_N - \delta_N = \frac{2r\delta_N}{(1-r)}$$

and

$$-2Nr^N\pi\omega_1(1+r) = \frac{1+r}{1-r}\delta_{N+1} + \delta_{N+1} = \frac{2\delta_{N+1}}{(1-r)}.$$

Observe that $\delta_{N+1} = r\delta_N$. We thus see a *period adding cascade* for which there is a sequence of disjoint intervals I_N, I_{N+1}, I_{N+2} etc., for which N is constant over the interval $\delta \in I_N$ and a $(\beta^N\gamma)$ orbit is observed. Furthermore if $\delta \in I_N$ then $\delta r \in I_{N+1}$. For a given $\delta > 0$ we may estimate N by solving the identity

$$-2Nr^N\pi\omega_1 = 2\delta/(1-r)$$

so that N grows like $\log(\delta)/\log(r)$ as $\delta \to 0$. As $W = 1/(N+1)$ it follows that

$$W \sim 1/|\log(\delta)| \quad \text{as} \quad \delta \to 0^+.$$

A schematic illustration of this analysis and the actual case is respectively given in Fig. 15(a) and (b), where we show the corresponding values of the b_n iterates of the $\beta-$map.
In Fig. 16 we compare b_n-iterations of the original system described in sec. 3 with the derived map in a vicinity of κ_C. These figures closely correspond, especially for large N, but show certain discrepancies close to the boundaries of the intervals I_N. The above analysis has used the approximation that the interval T is mapped to a

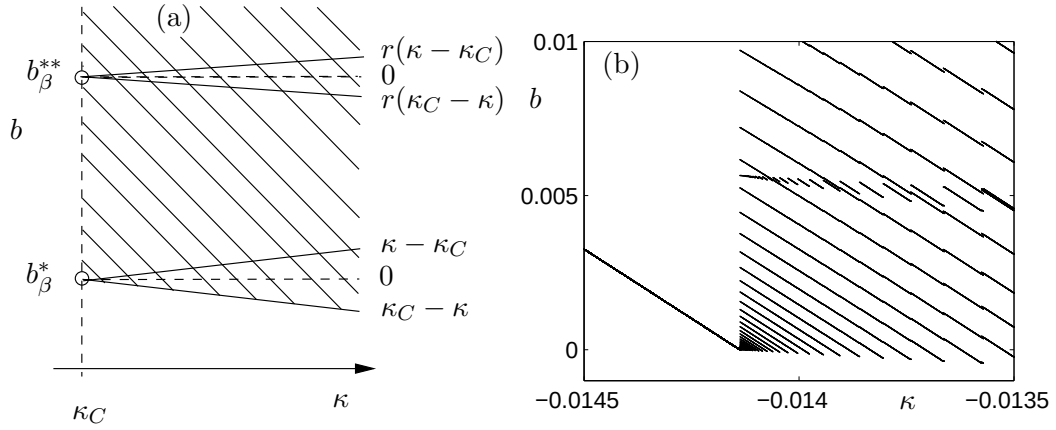

Figure 15: (a) A schematic showing the mechanisms behind the period adding phenomena. (b) Actual iterations of the $\beta-$map close to $\kappa_C = -0.014137$ for $\omega = 1.999$ and $r = 0.8$.

point by the iterations of the β map, whereas it is in fact mapped to a small interval. When this interval overlaps the end points of T we get more complex dynamics. For example, if $\delta \in I_N$ and δ is close to δ_{N+1} the corresponding return map F has two components, leading to a period-two point in T. This is equivalent to a $(\beta^N\gamma\beta^{N+1}\gamma)$ orbit of winding number $W = 2/(2N+3)$ lying between the $(\beta^{N+1}\gamma)$ orbit with $W = 1/(N+2)$ and the $(\beta^N\gamma)$ orbit with $W = 1/(N+1)$. In Fig.17(a) and (b) we give illustrations of two orbits ($(\beta^{11}\gamma)$ and $(\beta^{11}\gamma\beta^{12}\gamma)$) when $\kappa = -0.0127$ and $\kappa = -0.0128$, respectively, where $\omega = 1.999$ and $r = 0.8$.

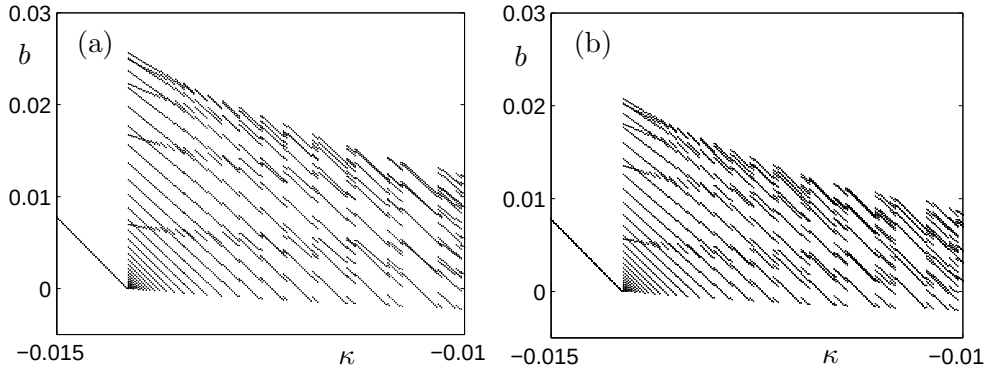

Figure 16: Iterations of b under κ variations using (a) direct numerical simulation of the original system and (b) the simplified 2D maps, where $\omega = 1.999$ $r = 0.8$.

The behaviour for small δ when $r < \phi$ is broadly similar to that when $r > \phi$ except that we see periodic orbits of the form $\beta^N\alpha$ for large N. An example of this is given in Fig. 18(a) and (b) for the case of $r = \phi - 0.002$ and $r = \phi + 0.002$, respectively. More generally if $r > \phi$ then as κ increases away from κ_β we see a transition from $\beta\gamma$ type dynamics to mixed $\alpha\beta\gamma$ dynamics and ultimately to $\alpha\beta$ dynamics as κ_1 approaches κ_α. The closer that r is to the value $r = \phi$ the smaller the range of values of κ_1 where we get only $\beta\gamma$ dynamics.

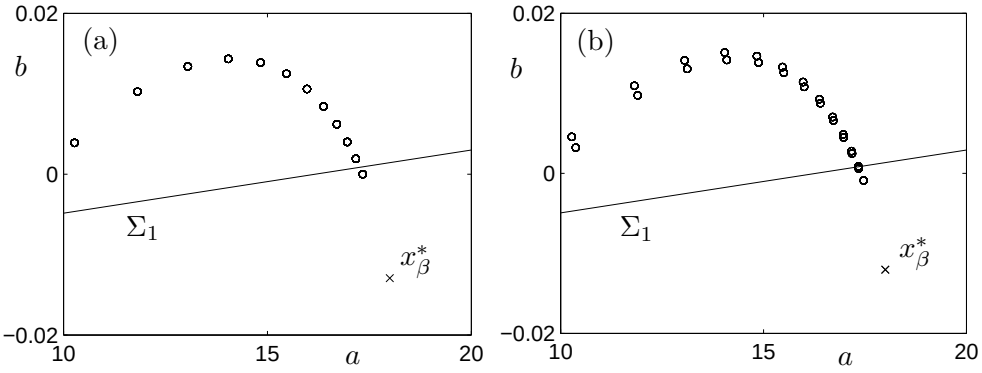

Figure 17: Periodic orbits for (a) $\kappa = -0.0127$ (b) $\kappa = -0.0128$. In both cases $r = 0.8$ and $\omega = 1.999$.

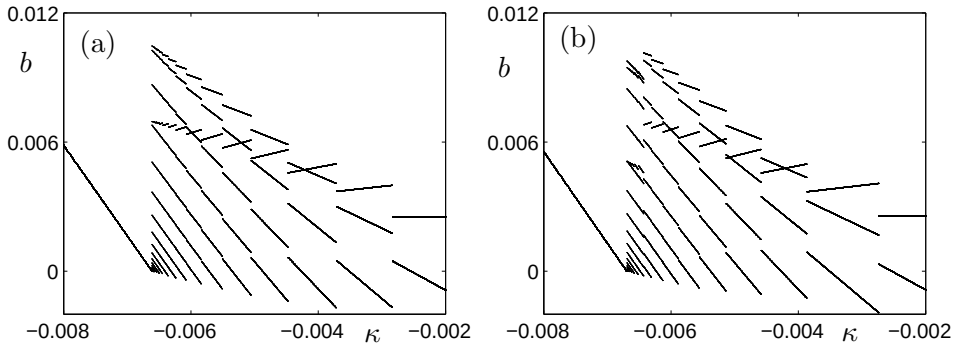

Figure 18: Bifurcation diagrams of the 2D maps for $\omega = 1.999$ and $r = 0.8$ showing b under κ variations when (a) $r = \phi - 0.002$ and (b) $r = \phi + 0.002$.

6 Systems of impact oscillators

6.1 The system studied

We now consider an application of this analysis to the difficult problem of the dynamics of a system of impact oscillators in the situation of a multiple impact.

As remarked in Section 2, the function $z(t) = \kappa + \beta|\sin(\omega t)|$ resembles the motion of a particle rebounding from a sinusoidally moving obstacle. In this interpretation we can consider the motion of the particle $u(t)$ induced by that of the obstacle $z(t)$ to be that of a light particle, rebounding from a much more massive particle $z(t)$ which is itself driven by a smoothly moving obstacle at position $w(t)$. A corner event then corresponds to a simultaneous impact between u, z and w.

In this section we carry this analogy further to make a numerical investigation of the motion of two particles at positions $z(t) < u(t)$ where $z(t)$ impacts with a smoothly moving obstacle at position $w(t) < z(t)$ and $u(t)$ impacts with $z(t)$. The dynamics following a simultaneous collision with $w = z = u$ is not well understood, but we show, through the numerical studies, that if the particle at z is very massive compared with the particle at u, that the motion is very similar to that of the

non-smoothly forced system close to a corner event.

We suppose that the smoothly moving obstacle is at the position

$$w(t) = \kappa + \beta \sin(\omega_0 t), \tag{72}$$

where $\kappa, \beta, \omega_0 \in \mathbb{R}$. We will also suppose that the motion of the particles at $z(t)$ and $u(t)$ is governed by the differential equations

$$\frac{d^2 z}{dt^2} + \omega_1^2 z = 0 \quad \text{and} \quad \frac{d^2 u}{dt^2} + \omega_2^2 u = 0, \tag{73}$$

respectively. Further, let the mass of the first particle be M and the mass of second particle m, and let the mass ratio between the two particles be

$$\mu = \frac{M}{m}.$$

An impact between the two free particles occurs at a time t if $z(t) = u(t)$. Let the positions of the particles before and after the impact be $z^{\pm}$ and $u^{\pm}$ and the velocities are $y^{\pm}$ and $v^{\pm}$ respectively. A reasonable model for the impact is that the combined momentum of the system is conserved but that the relative velocity is reversed and reduced by a factor r so that

$$u^+ = u^- = z^+ = z^-, \quad My^- + mv^- = My^+ + mv^+, \quad \left(v^+ - y^+\right) = -r\left(v^- - y^-\right).$$

Solving this system we have

$$\begin{pmatrix} z^+ \\ u^+ \\ y^+ \\ v^+ \end{pmatrix} = \begin{pmatrix} 1 & 0 & 0 & 0 \\ 0 & 1 & 0 & 0 \\ 0 & 0 & \frac{\mu - r}{1+\mu} & \frac{1+r}{1+\mu} \\ 0 & 0 & \frac{\mu(1+r)}{1+\mu} & \frac{1-r\mu}{1+\mu} \end{pmatrix} \begin{pmatrix} z^- \\ u^- \\ y^- \\ v^- \end{pmatrix}. \tag{74}$$

In the limit of $\mu \to \infty$ this reduces to the impact law(5). We will use the law(5) to describe the impacts between w and z. As a consequence the velocity y^- just before impact will, in general, be different from the velocity y^+ just after impact. For very large μ ($M \gg m$) we might expect to see behaviour of u close to that of the non-smoothly forced problem.

6.2 Observed dynamics

If $\omega_1 = \omega_2 = \beta = 1$, then when z is very massive compared to u by comparison with the simplified system in sec. 3 we might expect to have a triple impact leading to a corner bifurcation close to the parameter values of $\omega_0 = 2$, $\kappa = 0$. We show in Fig. 19 the dynamics observed in the case of $\mu = 1000$, $r = 0.8$, $\omega_1 = 1.001$, $\omega_2 = 1$ keeping $\kappa = 0$ fixed and varying ω_0. It is clear from this figure that the dynamics is relatively simple if $\omega_0 > \omega_C = 1.99975$ but becomes much more complex if $\omega_0 < \omega_C$. Indeed, we see the creation of a series of periodic orbits, with a period adding structure very similar to that observed for the single non-smoothly forced oscillator. Notice that there seem to be more attractors in this case than for the one impacting particle. The implication of this simple experiment is that the corner bifurcation structure observed when z is infinitely massive compared to u is preserved locally when z is large but finitely massive. Thus, the existence of a triple impact implies the creation

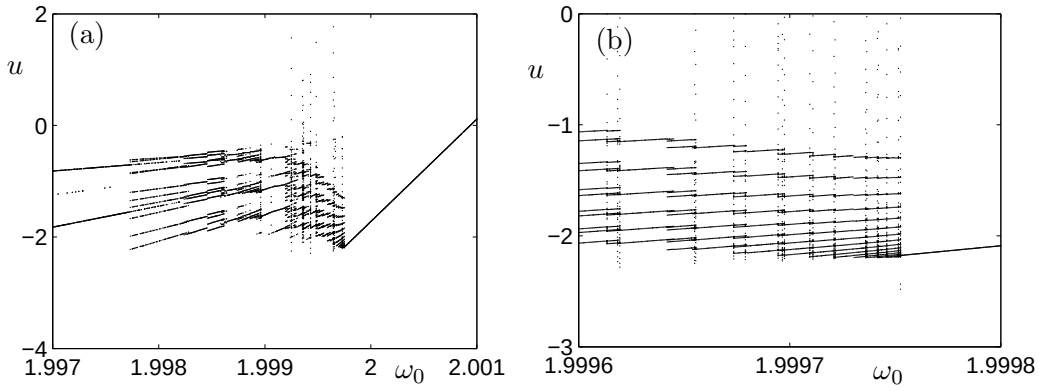

Figure 19: Bifurcation diagrams under ω_0 variations, where (b) is a zoom-in of (a) close to a corner bifurcation. Here $\omega_1 = 1.001$, $\omega_2 = 1$, $\kappa = 0$, $\beta = 1$ and $r_1 = r_2 = 0.8$.

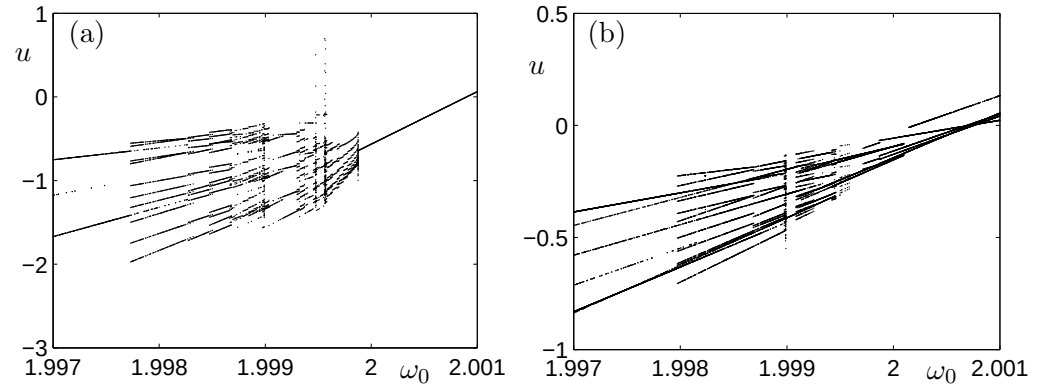

Figure 20: Bifurcation diagrams under ω_0 variations, for (a) $\mu = 100$ (b) $\mu = 10$. In both cases $\omega_1 = 1.001$, $\omega_2 = 1$, $\kappa = 0$, $\beta = 1$ and $r_1 = r_2 = 0.8$.

of a large number of new periodic orbits. This deduction clearly demonstrates the rich complexities of the dynamics likely to be observed when studying *systems* of impact oscillators.

In comparison, we plot in Fig. 20(a) and (b) the same scenario as in Fig. 19 but now with $\mu = 100$ and $\mu = 10$, respectively. In the first case ($\mu = 100$) we find that the bifurcation scenario has not changed significantly from $\mu = 1000$. However, in the second case ($\mu = 10$) the bifurcation diagram is clearly different and the corner bifurcation structure that was clearly visible before cannot be located. The number of attractors for $\omega_0 > \omega_C$ is higher than before which could explain why the sudden jump to high-periodic orbits cannot be seen.

All in all, this clearly shows the significance of the mass ratio and (again) the additional complexity that the increase in the number of impacting objects gives to the dynamical behaviour.

7 Summary and outlook

In this paper we have made a first attempt to study the effect of forcing an impact oscillator with a non-smooth forcing and linking this with the complex problem of multiple impacting systems between massive and light particles. By considering an infinitely massive particle to oscillates with a non-smooth motion given by $\kappa + |\sin(\omega t)|$, and analysing this problem close to a corner event at $\kappa = 0, \omega = 2$ it is possible to show that locally the dynamics can be studied in terms of locally have three piecewise linear maps. By using these maps we can also explain some of the dynamics close to a corner bifurcation under variations of κ and ω, such as the creation of an infinite number of periodic orbits through a period-adding cascade.

A possible application in which we might have a non-smoothly moving obstacle might be that of a valve rod rebounding from a cam, as illustrated in Fig. 21 (see also [13, 14]). Notice that the discontinuity is here greatly exaggerated. This example closely resembles the type of system that has been studied in this paper. In this case, the height $z(t)$ of the cam, in line with the valve rod, is a nonsmooth periodic function with corners rotating at angular velocity ω.

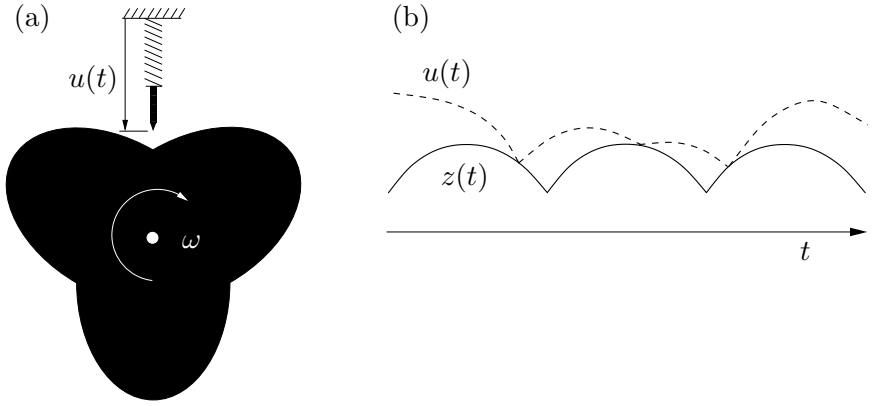

Figure 21: (a) A schematic of a rotating cam with angular velocity ω and a cam follower with position u. (b) A possible time history of the vertical positions of the cam and the follower.

Further, we have also looked at an example when we had two harmonically oscillating particles that impact each other and an oscillating rigid wall. As expected, when one particle is very massive compared to the other we saw a strong relationship between the behaviour after a triple collision and a corner bifurcation. However, much more work needs to be done to understand the dynamics of more general systems close to a triple impact.

Acknowledgment

The authors would like to acknowledge the support of the EU FP5 Project SICONOS (Grant no. IST-2001-37172).

References

[1] B. Azejczyk, T. Kapitaniak, J. Wojewoda, and R. Barron. Experimental-observation of intermittent chaos in a mechanical system with impacts. *J. Sound Vib.*, 178:272–275, 1994.

[2] V. I. Babitskii. *Theory of Vibro-impact Systems. Approximate methods*. Nauka, Moscow, 1978.

[3] P.V. Bayly and L.N. Virgin. An experimental study of an impacting pendulum. *Journal of Sound and Vibration*, 164(2):364–374, 1993.

[4] S.R. Bishop. Impact oscillators. *Phil. Trans. Roy. Soc. A*, 347:347–351, 1994.

[5] S.R. Bishop, M.G. Thompson, and S. Foale. Prediction of period-1 impacts in a driven beam. *Proc. Roy. Soc. Lond. A*, 452:2579–2592, 1996.

[6] P.C. Bressloff and J. Stark. Neuronal dynamics based on discontinuous circle maps. *Phys. Lett. A*, 150:187–195, 1990.

[7] C. Budd, K.A. Cliffe, and F. Dux. The effect of frequency and clearance varions on one-degree of freedom impact oscillators. *J. Sound & Vibration*, 184, 1995.

[8] C. J. Budd and F. Dux. Chattering and related behaviour in impact oscillators. *Phil. Trans. Roy. Soc. Lond. A*, 347:365–389, 1994.

[9] C. J. Budd and F. Dux. Intermittency in impact oscillators close to resonance. *Nonlinearity*, 7:1191–1224, 1994.

[10] C.J. Budd and A.G. Lee. Double impact orbits of periodically forced impact oscillators. *Proc. Roy. Soc. Lond. A*, 452, 1996.

[11] D.R.J. Chillingworth. Discontinuity geometry for an impact oscillator. *Dynamical Systems*, 17:380–420, 2002.

[12] W. Chin, E. Ott, H. E. Nusse, and C. Grebogi. Grazing bifurcations in impact oscillators. *Physical Review E*, 50:4427–4444, 1994.

[13] M. di Bernardo, G. Osorio, and S. Santini. Chattering and complex behavior behavior of a cam-follower system. In *Proceedings of European Nonlinear Oscillations Conference*, Eindhoven, The Netherlands, 2005.

[14] M. di Bernardo, G. Osorio, and S. Santini. Theoretical and experimental analysis of corner-impact bifurcations in a cam-follower impacting system. In preparation, 2005.

[15] S. Foale. Analytical determination of bifurcations in an impact oscillator. *Phil. Trans. Roy. Soc. London A*, 347:353–364, 1994.

[16] S. Foale and S. R. Bishop. Dynamical complexities of forced impacting systems. *Phil. Trans. Roy. Soc. London A*, 338:547–556, 1992.

[17] M. H. Frederiksson and A. B. Nordmark. Bifuractions caused by grazing incidence in many degrees of freedom impact oscillators. *Proc. Royal Soc. Lond. A*, 453:1261–1276, 1997.

[18] M. H. Fredriksson, D. Borglund, and A. B. Nordmark. Experiments on the onset of impacting motion using a pipe conveying fluid. *Nonlinear Dynamics*, 19:261–271, 1999.

[19] J. Guckenheimer and P. Holmes. *Nonlinear Oscillations, Dynamical Systems, and Bifurcations of Vector Fields*. Springer–Verlag, New York, 1983. Applied Mathematical Sciences, Volume 42.

[20] L. Higham. Nonlinear dynamics of piecewise linear maps. Master's thesis, University of Bristol, Department of Engineering Mathematics, 2000.

[21] S. J. Hogan, L. Higham, and T. C. L. Griffin. Dynamics of a piecewise linear map with a gap, 2005. In submission.

[22] A.P. Ivanov. Impact oscillations: linear theory of stability and bifurcations. *J. Sound Vib.*, 178:361–378, 1994.

[23] P. Jain and S. Banerjee. Border-collision bifurcations in one-dimensional discontinuous maps. *International Journal of Bifuraction and Chaos*, 13(11):3341–3351, 2003.

[24] J. P. Keener. Chaotic behaiviour in picewise continuous difference equations. *AMS Transactions*, 261:589–604, 1980.

[25] J. Molenaar, J.G. de Weger, and W. van de Water. Mappings of grazing-impact oscillators. *Nonlinearity*, 14, 2001.

[26] A.B. Nordmark. Non-periodic motion caused by grazing incidence in impact oscillators. *Journal of Sound and Vibration*, 2:279–297, 1991.

[27] A.B. Nordmark. *Grazing conditions and chaos in impacting systems*. PhD thesis, Royal Institute of Technology, Stockholm, Sweden, 1992.

[28] A.B. Nordmark. Universal limit mapping in grazing bifurcations. *Physical Review E*, 55:266–270, 1997.

[29] A.B. Nordmark. Existence of priodic orbits in grazing bifurcations of impacting mechanical oscillators. *Nonlinearity*, 14:1517–1542, 2001.

[30] M. Oestreich, N. Hinrichs, K. Popp, and C. J. Budd. Analytical and experimental investigation of an impact oscillator. In *Proc. of ASME 16th Biennal Conf. on Mech. Vibrations and Noise*, 1997.

[31] F. Peterka. Part 1: Theoretical analysis of n-multiple $(1/n)$-impact solutions. *CSAV Acta Technica*, 19:462–473, 1974.

[32] F. Peterka. Part 2: Results of analogue computer modelling of the motion. *CSAV Acta Technica*, 19:569–580, 1974.

[33] S.-X. Qu, S. Wu, and D.-R. He. A multiple devil's staircase in a discontinuous map. *Physics Letter A*, 231:152–158, 1997.

[34] S.-X. Qu, S. Wu, and D.-R. He. Multiple devil's staircase and type-V intermittency. *Physical Review E*, 57(1):402–411, 1998.

[35] K.N. Slade, L.N. Virgin, and P.V. Bayly. Extracting information from interimpact intervals in a mechanical oscillator. *Physical Review E*, 56(3):3705–3708, 1997.

[36] J.M.T. Thompson and R. Ghaffari. Chaotic dynamics of an impact oscillator. *Phys. Rev. A*, 27:1741–1743, 1983.

[37] J.M.T. Thompson and H.B. Stewart. *Nonlinear Dynamics and Chaos.* John Wiley and Sons, 1986.

[38] G. S. Whiston. Global dynamics of a vibro-impacting linear oscillator. *J. Sound Vib.*, 118:395–429, 1987.

[39] G. S. Whiston. The vibro-impact response of a harmonically excited and preloaded one-dimensional linear oscillator. *J. Sound Vib.*, 115:303–324, 1987.